Funk *et al.*

Chromosome 8 gain drives cancer progression by hijacking the translation factor 4E-BP1 sensitizing for targeted CDK4/6 inhibition

Cornelius M. Funk[1,2,3], Anna C. Ehlers[1,2,3], Martin F. Orth[4], Karim Aljakouch[5,6], Jing Li[1,2,3], Tilman L. B. Hölting[1,2,3,7], Rainer Will[8], Franziska Willis[9,10], Endrit Vinca[1,2,3], Shunya Ohmura[1,2,3], Roland Imle[2,3,11,12,13], Jana Siebenlist[1,2,3], Maximilian M. L. Knott[14,15], Felina Zahnow[1,2,3], Ana Sastre[16], Javier Alonso[17,18], Felix Sahm[19,20], Anna Loboda[2,3,13,21], Heike Peterziel[2,3,21], Martin Schneider[9,10], Ana Banito[2,3,11], Gabriel Leprivier[22], Wolfgang Hartmann[23], Uta Dirksen[24], Olaf Witt[2,3,21,25], Ina Oehme[2,3,21], Stefan M. Pfister[2,3,25,26], Laura Romero-Pérez[1,2,3,27,28], Jeroen Krijgsveld[5,13], Florencia Cidre-Aranaz[1,2,3], Thomas G. P. Grünewald[1,2,3,4,29,*,§], Julian Musa[1,2,3,9,10*]

* T.G.P.G. and J.M. share senior authorship

Author affiliations:
1 German Cancer Research Center (DKFZ) Heidelberg, Division of Translational Pediatric Sarcoma Research, Germany
2 Hopp Children's Cancer Center Heidelberg (KiTZ), Heidelberg, Germany
3 National Center for Tumor Diseases (NCT), NCT Heidelberg, a partnership between DKFZ and Heidelberg University Hospital, Germany
4 Max-Eder Research Group for Pediatric Sarcoma Biology, Institute of Pathology, Faculty of Medicine, LMU Munich, Munich, Germany
5 German Cancer Research Center (DKFZ) Heidelberg, Division of Proteomics of Stem Cells and Cancer, Germany
6 Medical Faculty, Heidelberg University, Heidelberg, Germany
7 Department of Medical Oncology, National Center for Tumor Diseases (NCT), Heidelberg, Germany
8 Cellular Tools Core Facility, German Cancer Research Center (DKFZ), German Cancer Consortium (DKTK), Heidelberg, Germany
9 Department of General, Visceral, and Transplantation Surgery, University Hospital Heidelberg, Heidelberg, Germany
10 Present address: Department of General, Visceral, Thoracic, and Transplantation Surgery, University Hospital Giessen and Marburg, Giessen, Germany
11 Soft-Tissue Sarcoma Junior Research Group, German Cancer Research Center (DKFZ), Heidelberg, Germany
12 Division of Pediatric Surgery, University Hospital Heidelberg, Heidelberg, Germany
13 Faculty of Biosciences, Heidelberg University, Heidelberg, Germany
14 Institute of Pathology, Faculty of Medicine, LMU Munich, Munich, Germany
15 Present address: Department of Neurobiology, Faculty of Life Sciences & Sagol School of Neuroscience, Tel Aviv University, Tel Aviv, Israel
16 Unidad Hemato-oncología Pediátrica, Hospital Infantil Universitario La Paz, Madrid, Spain
17 Pediatric Solid Tumour Laboratory, Institute of Rare Diseases Research (IIER), Instituto de Salud Carlos III, Madrid, Spain
18 Centro de Investigación Biomédica en Red de Enfermedades Raras, Instituto de Salud Carlos III (CB06/07/1009; CIBERER-ISCIII), Madrid, Spain
19 German Cancer Research Center (DKFZ) Heidelberg, Clinical Cooperation Unit Neuropathology, Germany
20 Department of Neuropathology, University Hospital Heidelberg, Heidelberg, Germany
21 German Cancer Research Center (DKFZ) Heidelberg, Clinical Cooperation Unit Pediatric Oncology, Germany
22 Institute of Neuropathology, University Hospital Düsseldorf, Medical Faculty, Heinrich Heine University, Düsseldorf, Germany
23 Division of Translational Pathology, Gerhard-Domagk-Institute of Pathology, University Hospital of Münster, Münster, Germany
24 Pediatrics III, West German Cancer Center, German Cancer Consortium site Essen, National Cancer Center (NCT) site Essen, University Hospital of Essen, Essen, Germany
25 Department of Pediatric Oncology, Hematology, Immunology and Pulmonology, Heidelberg University Hospital, Heidelberg, Germany
26 German Cancer Research Center (DKFZ) Heidelberg, Division of Pediatric Neurooncology, Germany
27 Division of Molecular Pathology of Sarcomas, Institute of Biomedicine of Sevilla (IBiS), Virgen del Rocio University Hospital/CSIC/University of Sevilla/CIBERONC, Seville, Spain
28 Department of Normal and Pathological Cytology and Histology, School of Medicine, University of Seville, Seville, Spain
29 Institute of Pathology, Heidelberg University Hospital, Heidelberg, Germany

§ Address for correspondence

Thomas G. P. Grünewald, MD, PhD

Division Head, Division of Translational Pediatric Sarcoma Research (B410)

German Cancer Research Center (DKFZ) & Hopp-Children's Cancer Center (KiTZ)

Im Neuenheimer Feld 280, 69210 Heidelberg, Germany

Phone +49-6221-42-3718

Email t.gruenewald@kitz-heidelberg.de

Word count: 3585 (excluding Abstract, Materials & Methods, and Figure Legends)

Display items: 4 Figures, 4 Supplementary Figures, 10 Supplementary Tables

Running title: Chromosome 8 gain sensitizing for CDK4/6 inhibition

Key words: Chromosome 8 gain, chromosome 8 amplification, chromosome 8 copy number variation, EIF4EBP1, 4E-BP1, Ewing sarcoma, CDK4/6 inhibitor, Palbociclib, Ribociclib

Funk *et al.*

ABSTRACT

Chromosome 8 (chr8) gains are common in cancer. However, their potential contribution to tumor heterogeneity is largely unexplored. Ewing sarcoma (EwS) is characterized by pathognomonic *FET::ETS* fusions, but show a general paucity of other recurrent somatic mutations that could explain the observed clinical diversity. In EwS, chr8 gains are the second most common genetic alteration rendering EwS an ideal model to investigate the relevance of chr8 gains in an otherwise silent genomic context.

Here, we report that chr8 gain-driven gene expression patterns correlate with poor overall survival of EwS patients. This effect is predominantly mediated by increased expression of the translation initiation factor binding protein 4E-BP1 encoded by *EIF4EBP1* on chr8. High *EIF4EBP1* expression showed the strongest association with poor overall patient survival among all chr8-encoded genes and correlated with chr8 gains in EwS tumors. Similar findings were made in numerous entities of The Cancer Genome Atlas (TCGA). In the EwS model, silencing of 4E-BP1 reduced cell proliferation, clonogenicity, spheroidal growth *in vitro*, and tumorigenesis *in vivo*. Integrated multi-omics profiling uncovered that 4E-BP1 orchestrates a multifunctional proteomic network including hubs affecting RNA processing, translational regulation, and chromatin modification. Drug screens and functional assays revealed that high 4E-BP1 expression sensitizes for pharmacological CDK4/6 inhibition in preclinical models.

Collectively, we establish chr8 gains and high 4E-BP1 expression as prognostic biomarkers in EwS and demonstrate that their association with poor patient outcome is primarily mediated by 4E-BP1 orchestrating a multifunctional proteomic network sensitizing EwS for CDK4/6 inhibitors. Our data suggest that testing for chr8 gain may improve risk-stratification and therapeutic management in EwS and other cancers.

Funk *et al.*

INTRODUCTION

Aneuploidy is common in cancer cells and plays an important functional role in their pathophysiology[1–3]. Copy number alterations of chr8, especially chr8 gains, are observed in numerous cancer entities, including EwS, acute/chronic myeloid leukemia, gastric cancer, myxoid liposarcoma, pediatric undifferentiated sarcoma, clear cell sarcoma, and malignant peripheral nerve sheath tumors[2,4–11]. However, the functional and clinical role of chr8 gains remains to be clarified. In the context of precision oncology, understanding the role of specific chromosomal gains and losses as a major source of inter-tumor heterogeneity is important for the development of novel personalized diagnostic and therapeutic approaches.

EwS is a malignant bone- and soft tissue-related tumor, primarily occurring in children, adolescents, and young adults[12]. It is characterized by a low number of recurrent somatic mutations and is driven by chromosomal translocations generating pathognomonic *FET::ETS* fusions, with *EWSR1::FLI1* being the most common (present in 85% of cases), encoding aberrant chimeric transcription factors[12]. Genetic variants in polymorphic enhancer-like DNA binding sites of EWSR1::FLI1 were shown to account for inter-individual heterogeneity in EwS susceptibility, tumor growth, clinical course, and treatment response[13–15]. Secondary somatic mutations in *STAG2* and *TP53* occur in approximately 20 and 5% of EwS patients[16–18], respectively. However, little is known about other, even more common recurrent alterations, such as chromosomal gains and/or losses, and their impact on inter-individual tumor heterogeneity.

Chr8 gain is present in approximately 50% of EwS cases, often in the form of chr8 trisomy, making it the second most frequently observed recurrent somatic alteration in EwS, following *FET::ETS* fusions[16–22]. Until now, studies have only addressed correlative specific aspects regarding the role of (partial) chr8 gains in EwS[16–19,21,23–28]. Consequently, the precise functional and clinical impact, particularly trisomies and whole chr8 gains, in EwS remains unclear. EwS serves as an ideal model to investigate the role of chr8 gain in cancer, given that EwS exhibit a 'silent' genome in which chr8 gains occur in an oligomutated genomic context[12].

Funk *et al.*

Therefore, the present study aimed to investigate the possible association between chr8 gains and tumor progression in the EwS model and to identify the most clinically relevant genes located on chr8 that may functionally contribute to inter-individual variability in patient outcomes. Following an integrative functional genomics approach, we have identified the eukaryotic translation initiation factor 4E binding protein 1 (EIF4EBP1, alias 4E-BP1) as the most promising chr8 candidate gene. It is outstandingly associated with unfavorable patient outcome compared to all other captured genes located on chr8 and even across the entire EwS transcriptome. 4E-BP1 functions downstream of its inactivating kinase complex, mTORC1 (mammalian target of rapamycin complex 1), and is a key effector of the mTORC1 signaling pathway[29,30]. 4E-BP1 belongs to a family of eIF4E-binding proteins that enable mTORC1 to adjust mRNA translation rates in response to various stimuli by modulating the assembly of the 48S translation pre-initiation complex. However, its role in tumor initiation/progression has not yet been defined[29]. We demonstrate that overexpression of *EIF4EBP1* is mediated by chr8 gain in primary EwS tumors. Furthermore, its RNAi-mediated knockdown in cell line models reduces EwS growth *in vitro* and *in vivo,* by influencing a multifunctional proteomic network. Thus, we establish an association between chr8 gain and tumor progression, mediated by 4E-BP1 in EwS. Drug screens and drug sensitivity assays *in vitro* and *in vivo* revealed that high 4E-BP1 expression sensitizes cells to targeted CDK4/6 inhibitor treatment with the FDA-approved drugs Palbociclib and Ribociclib. This discovery offers a new therapeutic strategy for tumors with chr8 amplification and 4E-BP1 overexpression.

RESULTS

Chromosome 8 gain drives overexpression of the clinically relevant translation initiation factor 4E-BP1 in EwS

To gain initial insights into the potential role of chr8 gain as a mediator of poor patient outcomes in EwS, we analyzed a cohort of 196 EwS samples for which matched microarray gene expression data and clinical data were available (henceforth referred to as 'Cohort 1'). We inferred a chr8 gene

4

Funk *et al.*

expression signature as a surrogate model for factual chr8 gain and performed a single-sample Gene

Set Enrichment Analysis (ssGSEA) followed by hierarchical clustering, assigning each patient to

either a high or low chr8 gene expression signature group (**Figure 1a**). To validate the inferred chr8

gene expression signature as an appropriate clustering model, we first determined differentially

expressed genes (DEGs) between the chr8 high and low gene expression signature clusters. We then

performed a Position Related Data Analysis (PREDA) to map respective DEGs to chromosomal

positions, demonstrating that the vast majority of DEGs map to chr8 (**Supplementary Figure 1a**).

Secondly, we analyzed genome-wide copy-number variation (CNV) data (inferred from DNA

methylation arrays) from an independent cohort of 100 EwS tumors for which matched gene

expression data from RNA-sequencing were available (henceforth referred to as 'Cohort 2'). This

analysis showed that clustering according to the chr8 gene expression signature accurately reflects

the presence of chr8 gain, as assessed by DNA methylation arrays (**Supplementary Figure 1b**).

Kaplan-Meier analysis in Cohort 1 revealed that high chr8 gene expression signature was associated

with shorter overall EwS patient survival (*P*=0.0137, **Figure 1b**). Strikingly, even when only

considering patients with localized disease (i.e., without evidence for metastasis at diagnosis), this

association remained significant (*P*=0.0309, **Figure 1b**), indicating that chr8 gain is functionally

involved in mediating an unfavorable disease phenotype. In support of this hypothesis, it is

intriguing that while chr8 gain is found only in approximately 50% of primary tumors, around 80%

of EwS cell lines, which are expected to be derived from highly aggressive tumor clones, exhibit

chr8 gains (mostly trisomies)[16–19,21,24–28]. Together, these findings suggest that genes located on chr8

contribute to aggressive cellular behavior and disease progression in EwS.

To identify genes located on chr8 that are strongly associated with overall survival of EwS patients,

we performed a batch-analysis within Cohort 1 calculating *P*-values for the association with overall

patient survival for every gene represented on the microarray using our custom code software GenEx

applying Mantel-Haenszel statistics (**Supplementary Table 1**). Analysis of all covered genes

located on chr8 highlighted that high *EIF4EBP1* expression showed the strongest association with

Funk *et al.*

overall survival (**Figure 1c**, **Supplementary Table 2**). Additionally, *EIF4EBP1* ranked within the top 15 survival associated genes genome-wide (**Figure 1c, Supplementary Table 1**). Indeed, high expression of *EIF4EBP1* significantly correlated with unfavorable overall survival of EwS patients (nominal $P<0.0001$, Bonferroni-adjusted $P=0.049$, **Figure 1d**). In keeping with the association of chr8 gain with poor overall survival, high *EIF4EBP1* expression remained significantly associated with poor patient overall survival even if the analysis was restricted to only patients with localized disease ($P=0.0013$, **Figure 1d**). Furthermore, *EIF4EBP1* expression is significantly correlated with high ssGSEA enrichment scores for chr8 gene expression ($P<0.001$, Pearson´s r = 0.47, Cohen´s d = 1.19), indicating that a significant part of the negative prognostic effect of high chr8 gene expression signature can be explained by high *EIF4EBP1* expression, and that gain of chr8 is significantly associated with higher *EIF4EBP1* expression in Cohort 2 ($P<0.001$; **Figure 1e**).

Interestingly, PREDA analysis of Cohort 1 revealed that *EIF4EBP1* seems to be distinctively differentially upregulated within genes of the mTOR signaling pathway that belong to the chr8 high gene expression signature group (**Supplementary Figure 1c**), indicating that 4E-BP1 has a distinct clinical and functional role within the mTOR signaling pathway in EwS.

To evaluate a potential clinical and functional role of chr8 gain and *EIF4EBP1* expression in other cancer entities beyond EwS, we analyzed CNV data from DNA methylation arrays of The Cancer Genome Atlas (TCGA). Our analysis revealed that numerous cancer entities exhibit chr8 gains (8 out of 32 identified entities exhibit chr8 gains in more than 10% of cases) at variable frequencies, and chr8 gain and high *EIF4EBP1* expression are associated with unfavorable patient survival in several other cancer entities (chr8 gain in 4 and high *EIF4EBP1* expression in 14 out of 32 identified entities), such as hepatocellular carcinoma, renal papillary cell carcinoma, lower-grade glioma, and thymoma (**Supplementary Table 3**).

Collectively, these results indicate that chr8 gain contributes to unfavorable EwS patient outcome and highlight 4E-BP1 as a potential driver of EwS aggressiveness encoded on chr8.

Funk *et al.*

4E-BP1 promotes EwS tumorigenicity *in vitro* and *in vivo*

In contrast to our findings that high *EIF4EBP1* levels significantly correlated with worse patient outcome (**Figures 1c,d**), and despite the complex role of 4E-BP1 in cancer, which strongly depends on the cellular context and its precise phosphorylation status[29], a recent report has suggested that 4E-BP1 may act as a tumor suppressor in EwS[31]. However, this conclusion was based on observations upon supraphysiological, ectopic overexpression of a phospho-mutant (and thus functionally inactive) 4E-BP1 protein in two EwS cell lines (EW8 and TC-71)[31]. To obtain a potentially more comprehensive view of 4E-BP1 in EwS and to generate first functional insights regarding its *in situ* role, we performed two pre-ranked fast Gene Set Enrichment Analyses (fGSEA) using gene expression data from Cohorts 1 and 2 by calculating Pearson's correlation coefficients between the mRNA expression levels of *EIF4EBP1* and those of every other gene represented in the respective dataset (**Supplementary Table 4,5**). Additionally, we carried out a third fGSEA using Cohort 1 by calculating the fold-changes (FCs) of all captured genes between tumors with and without predicted global chr8 gain (**Supplementary Table 6**). As an overlap between all three analyses, predominantly proliferation-associated gene sets were highly significantly positively enriched with predicted chr8 gain and *EIF4EBP1* expression at the mRNA level (**Figure 2a,b, Supplementary Table 4,5**). These transcriptomic data pointed toward a role of 4E-BP1 in the regulation of EwS cell proliferation and strongly supported the potential role of 4E-BP1 as a major mediator of chr8 gain-driven poor prognosis in EwS.

To further explore this hypothesis, we conducted functional experiments in EwS cell lines with relatively high *EIF4EBP1* expression levels (A-673, SK-N-MC, and TC-71) (**Supplementary Figure 2a**), two of which (SK-N-MC and TC-71) exhibit a chr8 gain[26]. To that end, we transduced EwS cell lines with a lentivirus containing a vector-system (pLKO Tet-on) with doxycycline (Dox)-inducible shRNAs, specifically directed against *EIF4EBP1* (sh4E-BP1_1 or sh4E-BP1_2) or a non-targeting control shRNA (shCtr). Both targeted shRNAs effectively silenced 4E-BP1 expression, as revealed by qRT-PCR and western blotting (**Supplementary Figure 2b–d**).

Funk *et al.*

Since *EIF4EBP1* expression levels appeared to correlate with pro-proliferative signatures in EwS tumors (**Figure 2a,b**), we carried out proliferation assays. Knockdown of 4E-BP1 for 96 h significantly inhibited cell proliferation in all three cell lines (**Figure 2c**). This anti-proliferative effect of 4E-BP1 knockdown appeared to be independent from cell death as Trypan-Blue-exclusion assays did not show a consistent significant effect of 4E-BP1 knockdown on cell death across all cell lines and shRNAs (**Supplementary Figure 2e**). In agreement with these short-term assays, prolonged 4E-BP1 knockdown (10–14 d) significantly reduced both 2D clonogenic and 3D anchorage-independent growth of EwS cells (**Figure 2d,e**). Such effects were not observed in shCtr cells (**Figure 2d,e**). Similarly, knockdown of 4E-BP1 significantly reduced growth of A-673 and TC-71 EwS cells subcutaneously xenotransplanted in flanks of NOD scid gamma (NSG) mice (**Figure 2f**, **Supplementary Figure 2f**). As expected from our in vitro findings, this phenotype was associated with a significantly diminished mitotic cell count, as revealed by histologic assessment of the respective xenografts (**Figure 2g, Supplementary Figure 2g**), whereas no difference in tumor necrosis was observed between xenografts with or without 4E-BP1 knockdown (**Supplementary Figure 2h,i**). To validate the effect of 4E-BP1 in an orthotopic xenograft model, TC-71 cells transduced with an inducible *EIF4EBP1* targeting shRNA construct (sh4E-BP1_2) were xenografted into the proximal tibia of NSG mice, which were subsequently treated with or without Dox. In accordance with our subcutaneous xenograft model, tumor burden in orthotopic EwS xenografts decreased upon Dox-induced knockdown of 4E-BP1 (**Supplementary Figure 2j**).

In summary and in conjunction with our findings from our patient data (**Figures 1b–d**), these functional preclinical data provide strong evidence that high 4E-BP1 expression promotes rather than suppresses EwS growth.

4E-BP1 guides a multifunctional proteomic network

As 4E-BP1 is a regulator of mRNA translation initiation, which binds to the translation initiation factor eIF4E and thereby modifies overall and selective translation rates[29], we performed proteomic

8

Funk *et al.*

profiling of newly synthesized proteins to gain mechanistic insights into how 4E-BP1 mediates its phenotype. We employed mass spectrometry (MS) to analyze the proteome of A-673, SK-N-MC, and TC-71 EwS cells with and without Dox-inducible shRNA-mediated knockdown of 4E-BP1 for 96 h (using respective cell lines with either two different specific shRNAs targeting *EIF4EBP1* or a non-targeting negative control shRNA), which were pulsed with stable isotope labeling by amino acids in cell culture (SILAC) media and the methionine analog L-Azidohomoalanine (AHA) for 6 h. To additionally identify proteins that may be indirectly regulated by 4E-BP1, i.e., at the transcriptional level, we paralleled our proteomic read-outs with transcriptome profiling of the same cells using gene expression microarrays. The MS analysis resulted in identification of 9,390 proteins, of which 4,800–7,200 proteins were quantified depending on the cell line. Those proteins that were only detected in one of the cell lines and those whose log$_2$FCs showed a standard deviation ≥0.5 between cell lines (empirically chosen cut-off) were not considered for further analyses, yielding 5,905 remaining proteins. Our microarray experiments captured 11,300 genes across all three cell lines. Following empirically chosen cut-offs, genes whose log$_2$FCs showed a standard deviation ≥0.5 between cell lines were not considered for further analyses (8,726 genes remaining). Proteins were only considered as being directly regulated by 4E-BP1 when their mRNA |log$_2$ FCs| were <0.4 (3,864 proteins remaining).

After identification of differentially expressed proteins upon 4E-BP1 knockdown, which were not regulated by 4E-BP1 at the mRNA level across all three cell lines and both targeted shRNAs, (**Supplementary Table 7**), a pre-ranked fGSEA and weighted correlation gene network analysis (WCGNA) were performed for C2 and C5 collections of gene sets from the Molecular Signatures Database (MSigDB). The WCGNA revealed multiple key hubs of 4E-BP1-regulated protein sets comprising a broad functional spectrum, such as translational regulation, RNA processing, and chromatin modification (**Figure 3a,b, Supplementary Table 8**). As our results from transcriptomic fGSEAs of primary EwS (**Figure 2 a,b**, **Supplementary Table 4,5**) and our functional data in EwS cell lines (**Figure 2c–g**) indicate a role of 4E-BP1 in mediating altered proliferation of EwS cells,

Funk *et al.*

the data from WCGNA of directly 4E-BP1-regulated proteins suggest that 4E-BP1 modulates a variety of functional pathways to control this observed phenotype (**Figure 3a,b, Supplementary Table 8**).

While these findings warrant further investigation, our results indicate that 4E-BP1 regulates a multifunctional proteomic network that may mediate its observed phenotype in EwS.

High 4E-BP1 expression sensitizes for CDK4/6 inhibitor treatment

To obtain initial insights into how to clinically exploit our findings, we conducted 3D culture drug screens in A673 EwS cells with/without knockdown of 4E-BP1 (**Supplementary Figure 3a**). The drug screens revealed the highest differential sensitivity of 4E-BP1 high expressing cells toward Ribociclib (**Supplementary Figure 3a**), an FDA-approved CDK4/6 inhibitor[32–35]. We validated these findings in 2D culture experiments using A673 EwS cells with/without knockdown of 4E-BP1, additionally using a second FDA-approved CDK4/6 inhibitor, Palbociclib (**Figure 4a**)[32–35]. Interestingly, EwS cell lines with high endogenous 4E-BP1 expression (A673 and TC-71) showed greater sensitivity to Palbociclib and Ribociclib than cell lines with low endogenous 4E-BP1 expression (EW-22 and CHLA-10) (**Figure 4b**).

Next, we conducted xenograft experiments by transplanting A673 EwS subcutaneously into the flanks of NSG mice, treated with/without Dox and with/without Palbociclib. Xenografts with 4E-BP1 knockdown and xenografts with Palbociclib treatment similarly exhibited a very strong reduction of tumor growth, which correlated with a strong decrease in histologically assessable viable tumor burden as compared to respective xenografts without 4E-BP1 knockdown or Palbociclib treatment (**Figure 4c,d**, **Supplementary Figure 3b**). Consistently, the xenografts of mice with 4E-BP1 knockdown or treatment with Palbociclib, for which histological material was obtainable, showed a lower number of mitoses per high-power field (**Figure 4e**). However, since the very strong growth-inhibitory effects of either 4E-BP1 knockdown or Palbociclib treatment alone precluded the assessment of a potential differential effect of 4E-BP1 expression on sensitivity

Funk *et al.*

toward Palbociclib in this model (**Figure 4c,d**, **Supplementary Figure 3b**), we turned for further validation to patient-derived real-world data. To this end, we analyzed gene expression and 3D drug sensitivity data from 14 EwS patient-derived short-term cultures treated with Palbociclib or Ribociclib in the context of the Individualized Therapy For Relapsed Malignancies in Childhood (INFORM) registry[36]. Strikingly, we found that high *EIF4EBP1* expression is indeed associated with higher sensitivity toward CDK4/6 inhibitor treatment (**Figure 4f**). In summary, these results suggest that 4E-BP1 may serve as a valuable predictive biomarker for clinical CDK4/6 inhibitors.

DISCUSSION

The data presented herein in the EwS model establish chr8 gain as an unfavorable prognostic factor, primarily mediated through the overexpression of the translation initiation factor 4E-BP1, which guides multifunctional proteomic signatures and sensitizes cells to targeted CDK4/6 inhibitor treatment.

In precision oncology, it is crucial to decipher mechanisms underlying inter-tumoral heterogeneity to refine diagnostic and therapeutic algorithms[14,37,38]. In this context, the identification of chr8 gain as a prognostic factor emphasizes the relevance of cytogenetic testing, which may help stratify patients into prognostic and/or therapeutic subgroups. Although chr8 trisomies are observed in approximately 50% of EwS patients, so far, only trends or moderate associations between whole chr8 gain (i.e., trisomies) and poor patient outcome have been observed[21,23–25,39–41]. Our data provide evidence of a significant association between a high chr8 gene expression signature and poor overall survival of EwS patients (**Figure 1b**). Importantly, this association remains statistically significant even when only considering patients with localized disease (**Figure 1b**). Therefore, chr8 gain, as assessed by cytogenetic testing or fluorescence in situ hybridization (FISH) or a high chr8 gene expression signature score (i.e., as assessed by ssGSEA), might serve as a prognostic biomarker for poor overall patient survival. Consequently, it could be particularly useful for stratifying patients with localized disease into different treatment groups.

11

Funk *et al.*

Interestingly, partial chr8 gain is observed in 48–78% of EwS family tumors, and specifically the gain of chr8p, where *EIF4EBP1* is located, has been shown to be associated with EwS relapse[39,42]. Functionally, as *MYC* is located on chr8, the expression of MYC has been suspected to mediate a potential effect of (partial) chr8 gains on patient outcome[10,39]. However, the expression of *MYC* was not significantly associated with overall EwS patient survival in our cohort of 196 primary EwS with matched clinical annotations (*P*=0.689, **Supplementary Figure 4a**, **Supplementary Table 1**). This suggests that the mechanisms underlying the association of chr8 gain with EwS aggressiveness are more complex than previously anticipated. In line with this notion, recent evidence has indicated that chr8 gain mitigates EWSR1::FLI1-induced replication stress via expression of RAD21 resulting in promotion of EwS tumorigenicity[23]. Nevertheless, high expression of *RAD21* did not reach a significant association with overall EwS patient survival in our cohort (*P*=0.174; **Supplementary Figure 4b, Supplementary Table 1**).

Our results are consistent with data from other cancer entities that have shown a prognostic/predictive value of chr8 gain, as for example in acute myeloid leukemia[6] and chronic myeloid leukemia[4,5]. Interestingly, chr8 gain is also observed in several specific other sarcoma entities, including myxoid liposarcoma[9], clear cell sarcoma[8], and pediatric undifferentiated sarcomas[10]. Partial gains or losses of chromosome 8 have been described in a broad range of cancer entities, such as prostate, lung, hepatocellular, and renal cell carcinoma[43–47]. In contrast to the reported data from EwS, in other cancer entities, chr8p losses are most frequently described to be associated with unfavorable clinical parameters[45,47,48]. In the case of chr8q, gains are most frequently described as having tumor promoting functions due to resulting *MYC* amplification[43,46,47,49]. However, in our dataset of 196 EwS patients, a clinical association between *MYC* expression and overall patient survival was not evident (**Supplementary Figure 4a**, **Supplementary Table 1**). Furthermore, other possible mechanisms of *EIF4EBP1* upregulation, apart from chr8 gains, have been described across cancer entities. For example, direct upregulation driven by differential transcription factors [14,50], may account for high 4E-BP1 expression levels in individual tumors.

Funk *et al.*

We demonstrate that high 4E-BP1 expression levels sensitize EwS cells to CDK4/6 inhibitor treatment with Palbociclib and Ribociclib (**Figure 4**). These drugs are FDA-approved for the treatment of hormone receptor positive, human epidermal growth factor receptor 2 (EGFR2, alias HER2) negative advanced or metastatic breast cancer, used in combination with an aromatase inhibitor in postmenopausal women[32–35]. In addition to their prognostic value in EwS (**Figure 1**), chr8 gain and 4E-BP1 expression might serve as predictive markers to subject EwS patients into a CDK4/6-inibitor sensitive and non-sensitive groups. Such tailored stratification of patients into specific targeted treatment groups with already FDA-approved drugs could significantly and promptly improve EwS patient outcome within the context of precision oncology. Notably, preclinical studies have shown that IGF-1R activation can mediated CDK4/6 inhibitor resistance[51]. As a result, a phase II clinical trial investigating the therapeutic efficacy of Palbociclib in combination with the IGF-1R inhibitor Ganitumab for patients with relapsed or refractory EwS was conducted[52]. In this study, the respective drug combination lacked adequate therapeutic activity, although a subgroup of patients showed prolonged stable disease[52]. However, this study did not include patient stratification based on predictive biomarkers. This gap might be addressed in future studies by incorporating predictive testing for chr8 gain and/or 4E-BP1 expression.

Collectively, our data suggest that chr8 gain plays an important prognostic role in EwS and that its functional effects on tumor progression are primarily driven by increased 4E-BP1 expression. Since chr8 gain occurs in approximately 50% of EwS cases, our results indicate that this chromosomal aberration is a major source of inter-tumoral heterogeneity in EwS. Consequently, further cytogenetic testing of EwS might offer a refinement of clinical management within the context of precision oncology.

Funk *et al.*

MATERIALS AND METHODS

Provenience of cell lines and cell culture conditions

Human EwS cell line A-673 (RRID:CVCL 0080) and human HEK293T cells (RRID:CVCL_0063) were purchased from American Type Culture Collection (ATCC). Human EwS cell line SK-N-MC (RRID:CVCL 0530) was provided by the German collection of Microorganisms and Cell cultures (DSMZ). Human EwS cell line TC-71 (RRID_CVCL_2213) was provided by the Children's Oncology Group (COG). All cell lines were grown at 37 °C and 5% CO_2 in humidified atmosphere in RPMI 1640 medium supplemented with stable glutamine (Biochrom), 10% tetracycline-free fetal calf serum (FCS) (Sigma-Aldrich), 100 U/ml penicillin (Biochrom), and 100 µg/ml streptomycin (Biochrom) was used to grow the cells. Cells were routinely examined by nested PCR for mycoplasma infection. Cell line purity and authenticity was confirmed by STR-profiling.

Nucleotide extraction, reverse transcription, and quantitative real-time PCR (qRT-PCR)

Genomic DNA from human cell lines was extracted with the NucleoSpin Tissue kit (Macherey-Nagel), plasmid DNA was extracted from bacteria with the PureYield kit (Promega). RNA was extracted with the NucleoSpin II kit (Macherey-Nagel) and reverse-transcribed using the High-Capacity cDNA Reverse Transcription kit (Applied Biosystems). qRT-PCR reactions were performed using SYBR green Mastermix (Applied Biosystems) mixed with diluted cDNA (1:10) and 0.5 μM forward and reverse primer (total reaction volume 15 μl) on a BioRad Opus instrument and analyzed using BioRad CFX Manager 3.1 software. Gene expression values were calculated using the $2^{-(\Delta\Delta Ct)}$ method[53] relative to the housekeeping gene *RPLP0* as internal control. Oligonucleotides were purchased from MWG Eurofins Genomics and are listed in **Supplementary Table 9.** The thermal conditions for qRT-PCR were as follows: initialization (95 °C, 2 min) (1 cycle); denaturation (95 °C, 10 sec), annealing (60 °C, 10 sec), and extension (60 °C, 10 sec) (49 cycles); denaturation (95 °C, 30 sec), annealing (65 °C, 30 sec), extension (melting curve 65 °C increasing 0.5 °C every 5 sec until 95 °C) (1 cycle).

Funk *et al.*

Generation of doxycycline (Dox)-inducible shRNA constructs

Human EwS cell lines A-673, SK-N-MC, and TC-71 were transduced with lentiviral Tet-pLKO-puro all-in-one vector system (plasmid #21915, Addgene) containing a puromycin-resistance cassette, and a tet-responsive element for Dox-inducible expression of shRNAs against *EIF4EBP1* (sh4E-BP1_1 or sh4E-BP1_2) or a non-targeting control shRNA (shCtr). Sequences of the used shRNAs are listed in **Supplementary Table 9**. Dox-inducible vectors were generated according to a publicly available protocol[54] using In-Fusion HD Cloning Kit (Clontech). Vectors were amplified in Stellar Competent Cells (Clontech) and respective integrated shRNA was verified by Sanger sequencing. The used sequencing primer is listed in **Supplementary Table 9**. Lentiviral particles were generated in HEK293T cells. Virus-containing supernatant was collected to infect the human EwS cell lines. Successfully transduced cells were selected with 1.5 μg/ml puromycin (InVivoGen). The shRNA expression for *EIF4EBP1* knockdown or expression of a negative control shRNA in EwS cells was achieved by adding 0.5 μg/ml Dox every 48 h to the medium. Generated cell lines were designated as A-673/TR/shCtr, A-673/TR/sh4E-BP1_1, A-673/TR/sh4E-BP1_2, SK-N-MC/TR/shCtr, SK-N-MC/TR/sh4E-BP1_1, SK-N-MC/TR/sh4E-BP1_2, TC-71/TR/shCtr, TC-71/TR/sh4E-BP1_1, and TC-71/TR/sh4E-BP1_2.

Western blot

A-673, TC-71, and SK-N-MC cells were treated for 96h with Dox to induce *EIF4EBP1* knockdown. Whole cellular protein was extracted with RIPA buffer (Serva electrophoresis) containing protease inhibitor cocktail and phosphatase inhibitor cocktail (Roche). Western blots were performed following routine protocols[55], and specific band detection was achieved by the use of rabbit monoclonal anti-4E-BP1 (clone Y329, 1:2,000, ab32024, Abcam) and rabbit polyclonal anti-p-4E-BP1 antibody (1:1,000, Ser65, #9451, Cell Signaling) and mouse monoclonal anti-ß-actin (1:5,000, A-5441, Sigma-Aldrich). Anti-rabbit IgG horseradish peroxidase coupled antibody (1:2,000, sc-

15

Funk *et al.*

516102, Santa Cruz Biotechnology) and anti-mouse IgG horseradish peroxidase coupled antibody (1:2,000, sc-2357, Santa Cruz Biotechnology) were used as secondary antibodies.

Proliferation assays

Depending on the cell line, $30–70 \times 10^3$ cells containing either a Dox-inducible non-targeting control shRNA or *EIF4EBP1*-targeting specific shRNAs were seeded in triplicate wells of a 6-well plate in 2 ml of growth medium. The cells were treated either with or without Dox (0.5 µg/ml; Sigma-Aldrich) for 120 h (medium was changed after 72 h including fresh Dox). Afterwards, cells of each treatment condition were harvested (including supernatant), stained with Trypan blue (Sigma-Aldrich), and viable as well as dead cells were counted in a standardized hemocytometer (C-chip, NanoEnTek). The assays were performed according to routine protocols[56].

Clonogenic growth assays (Colony forming assays)

Depending on the cell line, 500–1,000 cells containing either a Dox-inducible non-targeting control shRNA or *EIF4EBP1*-targeting specific shRNAs were seeded in triplicate wells of a 12-well plate in 2 ml of growth medium. Cells were grown with or without Dox (0.5 µg/ml) for 8–14 d depending on the cell line and afterwards stained with crystal violet (Sigma-Aldrich). Colony number and area was determined on scanned plates using Fiji (Image J)[57,58]. Clonogenicity index was calculated by multiplying the counted colonies with the corresponding colony volume.

Spheroidal growth assays

Depending on the cell line, 1,500–4,000 cells containing either a Dox-inducible non-targeting control shRNA or *EIF4EBP1*-targeting specific shRNAs were seeded in Costar Ultra-low attachment plates (Corning) for 8–14 d in 150 µl growth medium. To maintain the 4E-BP1 knockdown, 10 µl of fresh medium with or without Dox was added every 48 h to the cells. At day 8–14, the wells were photographed and spheres larger than 500 µm in diameter were counted. The

16

Funk *et al.*

area was measured using ImageJ. The sphere volumes were calculated as follows: $V = 4/3 \times \pi \times r^3$. The sphere index was calculated by multiplying the counted colonies with the corresponding colony volume.

Drug screening assays (3D)

Drug screening experiments were performed essentially as previously described in Peterziel et al.[59] using 384-well round bottom ultralow attachment spheroid microplates (# 3830, Corning) to allow the formation of three-dimensional spheroids.

Briefly, we tested a drug library of 75 drugs, mostly approved or in clinical trials, covering standard chemotherapeutic drugs, epigenetic modifiers, metabolic modifiers, kinase inhibitors, apoptotic modulators, and others[59–61]. Drug plates were ordered from FIMM High Throughput Biomedicine Unit (Institute for Molecular Medicine Finland HiLIFE, University of Helsinki, Finland) as ready-to-use assay plates and stored in an oxygen- and moisture-free environment (San Francisco StoragePod, Roylan Developments Ltd, Fetcham Leatherhead, UK) at room temperature until use. One drug plate set consisted of three plates. The concentration range of each drug covered five orders of magnitude with each condition tested in duplicate. Wells containing 100 µM benzethonium chloride (BztCl), 250 nM staurosporine (STS) (serving as a death control), and 0.1% DMSO were included as maximum, intermediate, and minimum effect controls, respectively. An STS concentration range of 0.1 to 1000 nM served as a technical control (two replicates per plate). Per well, 25 µl of single-cell suspension was dispensed on ready-to-use plates with an 8-channel electronic Picus® pipette (10 to 300 µl, #735361, Sartorius).

As a read-out for cell viability, bulk ATP quantitation with CellTiter-Glo® 2.0 (CTG; #G9243, Promega) to determine the relative number of metabolically active cells per well was performed 72 h after treatment according to the manufacturer´s protocol.

Prior to the drug screen, the suitable cell number to be seeded per well was determined by assessing the proportionality between the number of cells and the luminescence signal for 200, 500, 1000 and

Funk *et al.*

2,000 cells in the absence of drug treatment. The cell numbers used for the subsequent screening experiment were 250 cells per well for A-673 Dox (-) and 350 cells per well for A-673 Dox (+).

Drug effects were calculated as drug sensitivity scores (DSSasym) using the web-based drug analysis pipeline iTReX[61]. In analyses of Ribociclib and Palbociclib drug sensitivity screenings of primary patient cultures, a culture was considered as responsive if a drug sensitivity score ranged in the highest quartile, whereas samples ranging in the lower 3 quartiles were considered as non-responsive.

CDK4/6 inhibitor assays in vitro

A-673 and TC-71 (high endogenous 4E-BP1 expression) as well as CHLA-10 and EW-22 (low endogenous 4E-BP1 expression) EwS cells were seeded in a 96-well plate at a density of $0.5 - 2 \times 10^3$ per well. In case of cells containing Dox-inducible constructs, cells were treated with/without Dox (0.5 µg ml-1; Sigma-Aldrich). 48h after seeding or pre-incubation with Dox, respectively, CDK4/6 inhibitors (Palbociclib or Ribociclib; Biozol Diagnostica and Hölzel Diagnostika) were added in serially diluted concentrations ranging from 0.0032 to 500 µM. Each well contained an equal concentration of 0.5% DMSO (Sigma-Aldrich). Cells only treated with 0.5% of DMSO served as a control. After 72 h of inhibitor treatment, the plates were assayed on a GloMax® Explorer Multimode Microplate Reader after incubation with Resazurin (16 µg ml-1; Sigma-Aldrich) for 4-6 h.

Mass spectrometry (MS)

Pulse-Chase Labelling using AHA (azidohomoalanine) and SILAC isotope labels for nascent proteome analysis: A-673, SK-N-MC, and TC-71 EwS cells containing either a Dox-inducible non-targeting control shRNA or *EIF4EBP1*-targeting specific shRNAs (sh_4E-BP1_1 or sh_4E-BP1_2) were seeded at a density of 1×10^6 per 15-cm dish in 20 ml of culture medium and grown with or without Dox (0.5 µg/ml; Sigma-Aldrich) for 96h. Subsequently, cells were washed with pre-warmed

Funk *et al.*

PBS and cultivated in 10 ml SILAC RPMI deprivation media (lysine-, arginine-, and methionine-free) (Athenas) for 45 min at 37°C. This ensures the depletion of the intracellular stores of amino acid. The depletion medium was then aspirated and cells were incubated in 13 ml of SILAC RPMI pulse media containing 18.1 mg/l AHA (Jena Bioscience), and either 200 mg/l [13C6, 15N4] L-arginine and 40 mg/l [13C6, 15N2] L-lysine or 200mg/l [13C6] L-arginine and 40 mg/l [4,4,5,5-D4] L-lysine (Silantes) for 6h at 37°C with 5% CO_2. Following pulse labelling, cells were washed with PBS and harvested by scraping and centrifugation for 5 min at 400× g. Cell pellets were frozen and stored at –80°C until lysis. Enrichment of newly synthesized proteins for translatome analysis and sample preparation for LC-MS/MS measurements: Newly synthesized proteins were enriched using the Click-It alkyne agarose enrichment kit (Thermo Fisher) according to the manufacturer protocol with minor modifications. Cell pellets were lysed in 900 µl of Urea Lysis buffer (200 mM HEPES pH8, 0.5 M NaCl, 4% CHAPS, 8 M Urea), and cell lysates were sonicated on ice using the Benson probe sonicator. Protein concentrations were determined using the BSA kit (Thermo Fisher) and 1 mg of each label pair (+/– Dox) were mixed in a new tube. Volumes were made up to 1,700 µl end volume with 8M Urea lysis buffer. Next, the mixed lysates were combined with 100 µl of the alkyne-agarose slurry and 93 µl of the [3+2] cyclo-addition reaction mixture (10 µl Cu(II)SO4 (200 mM), 62.5 µl tris (hydroxypropyltriazolylmethyl) amine (THPTA, 160 mM), 10 µl aminoguanidine (2 M), 10 µl sodium ascorbate (2 M)), and incubated on a ThermoMixer for 2 h at 40°C. Following the incubation step, the resins were pelleted by centrifugation for 1 min at 2,000× *g* and supernatants were discarded. Subsequently, the resins were washed once with 2 ml of MQ water and pelleted by another centrifugation step. Next, the resins were resuspended in 2 ml of the 1-step reduction/alkylation mixture (10 mM Tris(2-carboxyethyl)phosphine, 40 mM 2-Chloroacetamide in SDS wash buffer) and incubated on a ThermoMixer for 15 min at 70 °C and another 15 min at 20 °C. Following the reduction/alkylation step, the resins were transferred into spin columns (BioRad) and placed on a P10 tip-box for the subsequent steps. The resins were consecutively washed five times with 1 ml SDS-Wash buffer (100 mM Tris-HCl pH 8.0, 1% SDS, 250 mM NaCl, 5 mM EDTA),

Funk *et al.*

once with MQ water, five times with Guanidine-Wash buffer (100 mM Tris-HCl pH 8.0, 6M Guanidine-HCl), and 5× with Acetonitrile-Wash buffer (20% Acetonitrile, ULCMS in Water ULCMS). Subsequently, the resins were resuspended in 200 µl Digestion buffer (100 mM Tris-HCl pH 8, 2 mM CaCl2, 5% Acetonitrile), transferred to new tubes, and subjected to proteolytic digestion by adding 1 µg of trypsin on a ThermoMixer for 16h at 37 °C. Following the digestion step, the resins were pelleted by centrifugation for 5 min at 2,000× g, the supernatants containing the digested peptides were transferred to new tubes and acidified with formic acid (FA) to 1% end concentration. For the peptide clean-up step, Oasis PRiME HLB µElution Plates (Waters) were used according to the manufacturer protocol. Briefly, the digested peptides were transferred to the Oasis plate and washed consecutively with 750 µl, 250 µl, and 100 µl of 1% FA. Peptides were eluted in a 96-well plate by adding 70 µl of elution solution (60% MeOH, 1% FA, 39% Water ULCMS) and another 50 µl of 100% MeOH. The eluted peptides were then dried down using a SpeedVac, resuspended in 0.1% TFA, and samples were subjected to HPLC fractionation and mass spectrometry analysis. LC-MS/MS analysis: Samples were analyzed on an Orbitrap Fusion mass spectrometer (Thermo Fisher) coupled with an Easy-nLC 1200 system (Thermo Fisher). Chromatographic separation was carried out using an Acclaim Pepmap RSLC trap column (100 µm × 2 cm, 5 µm particles, 100 Å pores, C18, Thermo Fisher), and nanoEase M/Z Peptide BEH analytical column, (75 µm × 250 mm, 1.7 µm particles, 130Å pores, C18, Waters). Peptides elution gradient was set to 105 min at flow rate of 300 nl/min using solvent A (0.1% formic acid in ULCM grade water) and solvent B (0.1% formic acid in 80% acetonitrile and 19.9% ULCM grade water). Samples were injected into the mass spectrometer using a 10 µm Picotip coated fused silica emitter (New Objective). The Orbitrap-Fusion mass spectrometer was operating in positive mode. Acquisition was carried out in data-dependent acquisition (DDA) mode. The MS1 scan was detected in orbitrap mode at 60,000 FWHM resolution, AGC target 1E6, scan range (m/z) was 375–1,500 DA, and maximal injection time was set to 50 ms. The intensity threshold HCD-fragmentation was set to 5E3. MS2 detection was acquired in centroid mode with an HCD collision energy of 33% in an ion trap detector, an isolation

20

Funk *et al.*

window (m/z) of 1.6 Da, AGC target 1E4, and maximal injection time of 50 ms. Data analysis: The raw files were analyzed using MaxQuant (version 1.6.10.43). The MS/MS spectra were searched through the integrated Andromeda search engine against Homo Sapiens UniProt proteome database. Multiplicity of labels was set to 3. Arg6/Lys4 and Arg10/Lys8 were selected as medium and heavy labels, respectively. Cysteine carbamidomethylation was selected for fixed modification. Methionine oxidation, protein N-terminal acetylation, replacement of methionine by AHA and conversion of AHA to homoserine (HS) and diaminobutyrate (DAB) were selected for variable modifications. Re-quantify and match between runs (match time window: 0.4 min) functions were enabled. For the digestion, Trypsin/P was selected, and the maximal number of mis-cleavages was set to 2. The minimal peptide length was set to 7 amino acids and FDR for peptide and protein identification was set to 0.01. For protein identification, at least one unique peptide was required. Minimum ratio count for label-based protein quantification was set to 2. Normalized H/M ratios derived from the ProteinGroups file were further processed and subjected to statistical analysis. FDR was set to >0.05 and S0 to 0.1. MS profiling was performed in biological triplicates for every cell line/construct/condition. For analysis of differential protein expression, $\log_2$ fold changes ($\log_2$FCs) between conditions with and without Dox treatment were calculated for every cell line, every construct, and every biological replicate. A mean $\log_2$FC across biological replicates was calculated for every cell line/construct and the mean $\log_2$FCs of both used specific shRNAs (sh_4E-BP1_1 and sh_4E-BP1_2) were summarized and normalized to that of the shCtr. Normalized $\log_2$ fold changes were summarized across cell lines. Proteins which were only detected in one of the cell lines and proteins whose $\log_2$FCs showed a standard deviation ≥0.5 between cell lines were not considered for further analyses. Proteins were only considered as being directly regulated by 4E-BP1 in case that their $\log_2$FCs at the mRNA level according to microarray profiling were within a $\log_2$FC between –0.4 and 0.4, implying that they are not regulated on mRNA level in a relevant manner. Cut-offs were chosen empirically.

Funk *et al.*

Xenotransplantation experiments

To assess local tumor growth of subcutaneous xenografts *in vivo*, 2.5×10^6 A-673 or TC-71 EwS cells containing either a Dox-inducible negative control shRNA or specific shRNAs against *EIF4EBP1* were injected subcutaneously with a 1:1 mix of PBS (Biochrom) and Geltrex (LDEV-Free Reduced Growth Factor Basement Membrane Matrix, Thermo Fisher Scientific; max volume 100 µl) in the right flanks of 4–8 week old NSG mice following routine protocols[62]. When tumors were first palpable, mice were randomized to the control group (17.5 mg/ml sucrose (Sigma-Aldrich) in drinking water) or the treatment group (2 mg/ml Dox Beladox, bela-pharm) and 50 mg/ml sucrose (Sigma-Aldrich) in drinking water. According to the average water intake of mice in the different treatment groups, the concentration of sucrose in the different treatment groups has been adapted: due to the bitter taste of Dox, the mice that receive Dox via their drinking water in average have a lower water intake, making a higher concentration of sucrose necessary to ensure equal intake of sucrose per mouse across the different treatment groups. Tumor size was measured with a calliper every two days and tumor volume was calculated as $V = a \times b^2 / 2$ with *a* being the largest diameter and *b* the smallest. Right before tumors reached the maximum size of 15 mm in one dimension (event), the respective mice were sacrificed by cervical dislocation. Other specific humane endpoints were determined as follows: invasive tumor growth leading to functional impairment or pain, ulcerating tumor (or fluid externalization), prolonged obstipation, abdominal distention, peritonitis, ascites, bloody diarrhea, palpable abdominal tumor mass with additional signs of pain, total relief, or medium paresis of a limb. General humane endpoints were determined as follows: Loss of 20% body weight, apathy, piloerection, self-isolation, aggressivity, automutilation, unphysiological or reduced movements/positioning, abnormal breathing, and reaching of a maximum observation period of 12 months.

For analysis of EwS xenograft growth in bone, TC-71/TR/sh4E-BP1_2 EwS cells were orthotopically injected into the proximal tibial plateau of NSG mice. One day before injection, mice were pre-treated with 800 mg/kg mouse weight/d Metamizole in drinking water as analgesia. On the

Funk *et al.*

day of injection, mice were anesthetized with inhaled isoflurane (2.5% in volume) and their eyes were protected with Bepanthen eye cream. After disinfection of the injection site, 2×10^5 cells/20 µl were directly injected with a 30 G needle (Hamilton) into the right proximal tibia. For pain prophylaxis after intraosseous injection, mice were treated with Metamizole in drinking water (800 mg/kg mouse weight/d). The first day after injection of tumor cells, mice were randomized in two groups of which one received henceforth 2 mg/ml Dox (BelaDox, Bela-pharm) dissolved in drinking water containing 5% sucrose (Sigma-Aldrich) to induce sh4E-BP1_2 expression, whereas the other group only received 5% sucrose. All mice were closely monitored routinely every two days and tumor growth was evaluated with a caliper. All tumor-bearing mice were sacrificed by cervical dislocation when the mice exhibited first signs of limping at the injected leg (event) or reached any humane endpoint as listed above.

For CDK4/6 inhibitor treatment *in vivo*, A-673/TR/sh4E-BP1_1 cells were injected subcutaneously as described above. As soon as the tumors were palpable, mice were subjected to either the vehicle (DSMO) or the treatment group (Palbociclib, (LC Laboratories), 100 mg kg-1), whereby each group was treated with or without addition of Dox to the drinking water (Beladox, bela-pharm, 2 mg ml-1). Palbociclib was administered by oral gavage for 28 days, with a break of 2 day every 5 days of treatment. The experimental endpoint was predetermined as 28 days after first injection of either inhibitor, or if humane endpoints as described above were reached before. To examine the number of mitoses within the tumors, hematoxylin and eosin (HE) stained slides of the respective tumors were examined and the number of mitoses were quantified as described below in section 'Histology'. Animal experiments were approved by the government of Upper Bavaria and North Baden and conducted in accordance with ARRIVE guidelines, recommendations of the European Community (86/609/EEC), and United Kingdom Coordinating Committee on Cancer Research (UKCCCR) guidelines for the welfare and use of animals in cancer research.

Funk *et al.*

Methylation arrays and CNV analysis

A minimum of 500 ng of high-quality DNA from 100 EwS FFPE samples was used for methylation and CNV analysis with the Infinium Human Methylation 450K BeadChip (EPIC array; Illumina). This method can analyze 864,928 CpGs including main CpG islands and CpG sites outside of CpG islands. Raw methylation and CNV data were essentially processed as previously reported[63]. Based on the methylome, we used a previously described sarcoma classifier[63], which assigns a score to each sample indicating the similarity of the respective methylome with methylation patterns of samples from known entities. CNVs were also assessed by this method and analyzed at both, chromosomal and specific locus level. Scores for specific positions were visualized in the Integrative Genomic Viewer (IGV).

For analysis regarding the association between chr8 gain and *EIF4EBP1* expression (as assessed by RNA-seq), only samples were analyzed which were clearly possible to separate into either a group showing global chr8 gain or no chr8 gain. Samples with partial gain were not considered.

For determining chr8 CNV status in tumor entities other than EwS we analyzed TCGA SNP array 6.0 pre-segmented data using TCGAbiolinks R library (Masked Copy Number segment, GRCh38.p0). We applied re-segmentation algorithm by CNApp[64] to classify samples as chr8 gain or no chr8 gain. Classification criteria for whole chr8 gain were log2 segment mean > 0.2 and the sum of all gained segments spanning ≥ 90% of total chr8 length. Whole chr8 gain frequencies were visualized for each entity individually as pie charts. To compare both groups (chr8 gain vs. no chr 8 gain) regarding overall patient survival we performed a Kaplan Meier analysis, in which significance levels were calculated using a log-rank test.

For determining chr8 CNA status in tumor entities other than EwS we analyzed TCGA SNP array 6.0 pre-segmented data using TCGAbiolinks R package[65] (Masked Copy Number segment, GRCh38.p0). For downstream analysis we selected all primary tumor samples for which clinical annotation was complete and SNP array and RNA sequencing (RNA-seq) datasets existed, we applied re-segmentation algorithm by CNApp[64] to classify samples as chr8 gain or no gain.

Funk *et al.*

Classification criteria for whole chr8 gain were log2 segment mean > 0.2 and the longest segment spanning ≥ 75% of total chr8 length (chr8q length 68%). To compare both groups (chr8 gain vs. no gain) regarding overall patient survival we performed a Kaplan Meier analysis using survival R package[66,67]. Significance levels were calculated using the log-rank test.

RNA sequencing (RNA-seq)

RNA quality was assessed by the Agilent 2100 Bioanalyzer (Agilent Technologies) before library preparation. 2 μg of estimated high-quality RNA were prepared for sequencing. Libraries were prepared according to the TruSeq RNA Exome (Illumina) protocol. Library preparation workflow included purification and fragmentation of mRNA, first and second strand cDNA synthesis, end repair, 3´ends adenylation, adapters ligation, PCR amplification, library quantification, normalization and libraries pooling. Cleanup cycles are introduced between the mentioned steps. Sequencing was performed on a NextSeq 550 / NovaSeq 600 Sequencer (Illumina). NextSeq 550 was performed with 75 bp 'paired-end' sequencing technology employing high-output flow cells. Calculations of RNA counts were performed as previously described[68,69].

Gene expression microarrays

A-673, TC-71, and SK-N-MC EwS cells containing either a Dox-inducible non-targeting control shRNA (shCtr) or *EIF4EBP1*-targeting specific shRNAs (sh4E-BP1_1 or sh4E-BP1_2) were seeded in T25 flasks (TPP) and treated either with or without Dox (0.5 μg/ml; Sigma-Aldrich) for 96h. Thereafter, total RNA was extracted from one biological replicate for each condition with the Nucleospin II kit from Machery-Nagel and transcriptome profiled at IMGM laboratories (Martinsried, Germany). RNA quality was assessed with a Bioanalyzer and samples with RNA integrity numbers (RIN) > 9 were hybridized to Human Affymetrix Clariom D microarrays. Data were quantile normalized with Transcriptome Analysis Console (v4.0; Thermo Fisher Scientific) using the SST-RMA algorithm. Annotation of the data was performed using the Affymetrix library

Funk *et al.*

for Clariom D Array (version 2, human) at the gene level. Differentially expressed genes across shRNAs and cell lines were identified as follows: First, normalized gene expression signal was $\log_2$ transformed. To avoid false discovery artifacts due to the detection of only minimally expressed genes, we excluded all genes with a lower or just minimally higher gene expression signal than that observed for *ERG*, which is known to be virtually not expressed in *EWSR1::FLI1* positive EwS cell lines[18]. A mean $\log_2$FC was calculated for every cell line/construct and the mean $\log_2$FCs of both used specific shRNAs (sh_4E-BP1_1 and sh_4E-BP1_2) were summarized and normalized to that of the shCtr. Normalized $\log_2$FCs were summarized across cell lines. Genes showing a standard deviation of ≥0.5 between 3 cell lines were not considered for further analysis.

Analysis of publicly available gene expression data and patient survival analysis

Microarray data of 196 EwS tumors (Cohort 1) (GSE63157, GSE34620, GSE12102, GSE17618 and unpublished data[70–73]) for which well-curated clinical annotations were available were downloaded from the Gene Expression Omnibus (GEO). The data were either generated on Affymetrix HG-U133Plus2.0 or on Affymetrix HuEx-1.0-st microarray chips and were normalized separately by RMA using custom brainarray chip description files (CDF, v20) as previously described[74]. Batch effects were removed using ComBat[75]. Tumor purity was calculated using ESTIMATE[76] and only samples with a tumor purity >60% corresponding to The Cancer Genome Atlas (TCGA) standard (http://cancergenome.nih.gov/cancersselected/biospeccriteria) were kept for further analyses. Samples were stratified by their quartile intra-tumoral gene expression levels. Significance levels were calculated with a Mantel-Haenszel test (calculated using GraphPad Prism version 9). *P*-values <0.05 were considered as statistically significant.

For analyzing the effect of *EIF4EBP1* expression level on clinical outcome in tumor entities other than EwS we analyzed TCGA RNASeq unnormalized counts data using TCGAbiolinks R package[65] (STAR - Counts, GRCh38.p0). For downstream analysis we selected all primary tumor samples for which clinical annotation was complete and SNP array and RNASeq datasets existed. We kept all

Funk *et al.*

genes with at least 50% samples showing counts greater than 0. Using DESeq2[77] for downstream analysis we applied variance stabilizing transformation algorithm on the counts matrix to produce normalized counts on the log2 scale. To investigate the association between *EIF4EBP1* expression and overall patient survival we performed Kaplan Meier analyses using the best percentile approach[66]. To determine the optimal threshold based on *EIF4EBP1* expression as a continuous variable (vst-counts), we used maximally selected rank statistics from the maxstat R package[78]. Significance levels were calculated using the log-rank test.

Fast gene-set enrichment analysis (fGSEA) and single-sample GSEA (ssGSEA)

fGSEA was performed using the FGSEA R package (v 4.1.3) based on Gene Ontology (GO) biological processes terms from MSigDB (c5.all.v7.5.1 symbols.gmt, c2.all.v7.5.1 symbols.gmt) and GO terms were filtered for statistical significance (adjusted $P<0.05$) (10,000 permutations)[79,80]. Using the Affymetrix gene expression dataset comprising 196 EwS patients (Cohort 1), enrichment of gene sets that are among *EIF4EBP1* co-regulated genes were identified by ranking of Pearson´s correlation coefficient of the expression of each gene with *EIF4EBP1* expression and performance of a pre-ranked fGSEA.

Using the RNA-seq gene expression dataset comprising 100 primary EwS patients (Cohort 2), enrichment of gene sets that are among *EIF4EBP1* co-regulated genes and among chr8 regulated genes were identified by performing a pre-ranked fGSEA on a) ranked Pearson´s correlation coefficient between the expression of each gene with *EIF4EBP1* expression and on b) ranked mean $\log_2 FC$ as calculated for each gene between the group of EwS with and without chr8 gain.

Employing an integrated dataset inferred from MS protein expression data and microarray gene expression data of A-673, SK-N-MC, and TC-71 EwS cell lines with/without 4E-BP1 knockdown containing differentially expressed proteins upon 4E-BP1 knockdown, all proteins were ranked by their mean $\log_2 FC$ and a pre-ranked fGSEA was performed.

Funk *et al.*

For inferring chr8 gene enrichment from gene expression data we applied single sample GSEA (ssGSEA)[81,82] on a EwS patient cohort of 196 tumor samples (Cohort 1) using gene sets from Ensembl 103 genes in cytogenetic band chr8 (Molecular Signatures Database (v7.4 MSigDB/c1.all.v7.5.symbols.gmt)). Genes considered for chr8 gene expression signature are listed in **Supplementary Table 10**. Based on the enrichment levels (ssGSEA scores) of chr8 we performed hierarchical clustering (pheatmap R package, version 1.0.12, https://cran.r-project.org/web/packages/pheatmap/pheatmap.pdf) to divide the EwS samples into a chr8 high and low gene expression group. To compare both groups regarding overall patient survival we performed a Kaplan Meier analysis. Significance levels were calculated with Mantel-Haenszel test (GraphPad Prism version 9).

Position Related Data Analysis (PREDA)

To validate appropriate clustering of Cohort 1 tumor samples into chr8 high and low gene expression groups we determined differentially expressed genes (DEGs) between both clusters using Limma[83] and Position Related Data Analysis (PREDA)[84] on iDEP[85] platform to map respective DEGs (FDR cut-off < 0.01) onto chromosomes. Using the Limma package[83], also DEGs of the mTOR signaling pathway were depicted.

Weighted gene correlation network analysis (WGCNA)

To construct a network, the WGCNA R package was used[53]. Briefly, a binary matrix of GO-/CCP-/CP-terms × genes (where 1 indicates the gene is present in the GO-/CCP-/CP-term and 0 indicates it is not) was created. Then, the Jaccard's distance for all possible pairs was computed to create a symmetric GO/CCP/CP adjacent matrix. Clusters of similar GO-/CCP-/CP-terms were identified using dynamicTreeCut algorithm, and the top 20% highest edges were selected for visualization. The highest scoring node in each cluster was determined as the cluster label (rName). The obtained

Funk *et al.*

network and nodes files were fed into Cytoscape (v 3.8.0) for network design and visualization as previously described[86].

Histology

HE-staining of EwS xenografts was performed according to routine protocols. Mitoses of EwS xenografts were quantified in HE-stained slides by two blinded observers in 5 high-power fields per sample. Mitoses per sample were determined by mean of total 10 counted high-power fields across both observers.

Statistics and software

Statistical data analysis was performed using GraphPad PRISM 9 (GraphPad Software Inc., CA, USA) on the raw data. If not otherwise specified in the figure legends comparison of two groups in functional *in vitro* experiments was carried out using a two-tailed Mann–Whitney test. If not otherwise specified in the figure legends, data are presented as dot plots with horizontal bars representing means, and whiskers representing the standard error of the mean (SEM). Sample size for all *in vitro* experiments were chosen empirically with at least 3 biological replicates. In Kaplan-Meier overall survival analyses, curves were calculated from all individual survival times of patients. Curves were compared by Mantel-Haenszel test to detect significant differences between the groups. For batch analyses of patient survival, the in-house custom code software GenEx was used, using the Mantel-Haenszel test for *P*-value calculation. Pearson´s correlation coefficients were calculated using Microsoft Excel or GraphPad PRISM 9 (GraphPad Software Inc., CA, USA). For *in vivo* experiments, sample size was predetermined using power calculations with $\beta = 0.8$ and $\alpha = 0.05$ based on preliminary data and in compliance with the 3R system (replacement, reduction, refinement). Kaplan-Meier analyses of event-free survival (*in vivo* experiments) were carried out using GraphPad PRISM 9 (GraphPad Software Inc.). The definition of the type of events is given in

Funk *et al.*

the corresponding figure legends, but generally corresponds to humane experimental endpoints as defined above.

30

Funk *et al.*

AUTHOR CONTRIBUTIONS

C.M.F. performed functional in vitro and in vivo experiments, as well as bioinformatic and histological analyses, analyzed and interpreted all data, designed all figures, and wrote the paper. M.F.O. performed functional experiments, helped in shRNA design and lentiviral transduction of cell lines. K.A. performed MS and analyzed MS data. A.C.E. performed bioinformatic analyses. J.S. helped in dataset curation. J.L. helped in conduction of *in vivo* experiments. T.L.B.H., M.M.L.K., E.V. assisted in experimental procedures. R.W. performed cloning of vectors. F.W. performed analyses of histology. F.Z. assisted in experimental procedures. S.O., R.I., A.B. helped in performance of *in vivo* experiments. J.A., A.S., W.H., U.D. provided clinical information. M.S. provided financial support and laboratory infrastructure. O.W., I.O., H.P., and A.L. performed drug screens. S.M.P., G.L. provided biological and technical guidance. L.R.-P. conducted methylation arrays and performed bioinformatic analyses. J.K. provided financial support and laboratory infrastructure for performance of MS. F.-C.A. carried out functional *in vitro* and *in vivo* experiments. J.M. coordinated and supervised the study, provided biological and technical guidance, performed functional experiments as well as bioinformatic and histological analyses, analyzed and interpreted all data, wrote the paper, and provided financial support. T.G.P.G designed, coordinated, and supervised the study, provided biological and technical guidance, analyzed and interpreted all data, wrote the paper and provided financial support and laboratory infrastructure. All authors read and approved the final manuscript.

CONFLICT OF INTEREST

We declare no conflicts of interest.

Funk *et al.*

REFERENCES

1. Ben-David, U. & Amon, A. Context is everything: aneuploidy in cancer. *Nat. Rev. Genet.* **21**, 44–62 (2020).

2. Gordon, D. J., Resio, B. & Pellman, D. Causes and consequences of aneuploidy in cancer. *Nat. Rev. Genet.* **13**, 189–203 (2012).

3. Vasudevan, A. *et al.* Aneuploidy as a promoter and suppressor of malignant growth. *Nat. Rev. Cancer* **21**, 89–103 (2021).

4. Wang, W. *et al.* Impact of trisomy 8 on treatment response and survival of patients with chronic myelogenous leukemia in the era of tyrosine kinase inhibitors. *Leukemia* **29**, 2263–2266 (2015).

5. Wang, W. *et al.* Clinical significance of trisomy 8 that emerges during therapy in chronic myeloid leukemia. *Blood Cancer J.* **6**, e490 (2016).

6. Wolman, S. R., Gundacker, H., Appelbaum, F. R., Slovak, M. L., & Southwest Oncology Group. Impact of trisomy 8 (+8) on clinical presentation, treatment response, and survival in acute myeloid leukemia: a Southwest Oncology Group study. *Blood* **100**, 29–35 (2002).

7. Panani, A. D., Ferti, A. D., Avgerinos, A. & Raptis, S. A. Numerical aberrations of chromosome 8 in gastric cancer detected by fluorescence in situ hybridization. *Anticancer Res.* **24**, 155–159 (2004).

8. Mrózek, K., Karakousis, C. P., Perez-Mesa, C. & Bloomfield, C. D. Translocation t(12;22)(q13;q12.2-12.3) in a clear cell sarcoma of tendons and aponeuroses. *Genes. Chromosomes Cancer* **6**, 249–252 (1993).

9. Sreekantaiah, C., Karakousis, C. P., Leong, S. P. & Sandberg, A. A. Trisomy 8 as a nonrandom secondary change in myxoid liposarcoma. *Cancer Genet. Cytogenet.* **51**, 195–205 (1991).

10. Selvarajah, S. *et al.* Characterization of trisomy 8 in pediatric undifferentiated sarcomas using advanced molecular cytogenetic techniques. *Cancer Genet. Cytogenet.* **174**, 35–41 (2007).

11. Dehner, C. *et al.* Chromosome 8 gain is associated with high-grade transformation in MPNST. *JCI Insight* **6**, e146351, 146351 (2021).

12. Grünewald, T. G. P. *et al.* Ewing sarcoma. *Nat. Rev. Dis. Primer* **4**, 5 (2018).

13. Grünewald, T. G. P. *et al.* Chimeric EWSR1-FLI1 regulates the Ewing sarcoma susceptibility gene EGR2 via a GGAA microsatellite. *Nat. Genet.* **47**, 1073–1078 (2015).

14. Musa, J. *et al.* Cooperation of cancer drivers with regulatory germline variants shapes clinical outcomes. *Nat. Commun.* **10**, 4128 (2019).

15. Machiela, M. J. *et al.* Genome-wide association study identifies multiple new loci associated with Ewing sarcoma susceptibility. *Nat. Commun.* **9**, 3184 (2018).

16. Tirode, F. *et al.* Genomic landscape of Ewing sarcoma defines an aggressive subtype with co-association of STAG2 and TP53 mutations. *Cancer Discov.* **4**, 1342–1353 (2014).

17. Brohl, A. S. *et al.* The genomic landscape of the Ewing Sarcoma family of tumors reveals recurrent STAG2 mutation. *PLoS Genet.* **10**, e1004475 (2014).

18. Crompton, B. D. *et al.* The genomic landscape of pediatric Ewing sarcoma. *Cancer Discov.* **4**, 1326–1341 (2014).

19. Mugneret, F., Lizard, S., Aurias, A. & Turc-Carel, C. Chromosomes in Ewing's sarcoma. II. Nonrandom additional changes, trisomy 8 and der(16)t(1;16). *Cancer Genet. Cytogenet.* **32**, 239–245 (1988).

20. Maurici, D. *et al.* Frequency and implications of chromosome 8 and 12 gains in Ewing sarcoma. *Cancer Genet. Cytogenet.* **100**, 106–110 (1998).

21. Armengol, G. *et al.* Recurrent gains of 1q, 8 and 12 in the Ewing family of tumours by comparative genomic hybridization. *Br. J. Cancer* **75**, 1403–1409 (1997).

22. Nacev, B. A. *et al.* Clinical sequencing of soft tissue and bone sarcomas delineates diverse genomic landscapes and potential therapeutic targets. *Nat. Commun.* **13**, 3405 (2022).

23. Su, X. A. *et al.* RAD21 is a driver of chromosome 8 gain in Ewing sarcoma to mitigate replication stress. *Genes Dev.* **35**, 556–572 (2021).

24. Tarkkanen, M. *et al.* Clinical correlations of genetic changes by comparative genomic

Funk *et al.*

hybridization in Ewing sarcoma and related tumors. *Cancer Genet. Cytogenet.* **114**, 35–41 (1999).

25. Hattinger, C. M. *et al.* Prognostic impact of chromosomal aberrations in Ewing tumours. *Br. J. Cancer* **86**, 1763–1769 (2002).

26. Orth, M. F. *et al.* Systematic multi-omics cell line profiling uncovers principles of Ewing sarcoma fusion oncogene-mediated gene regulation. *Cell Rep.* **41**, 111761 (2022).

27. Mackintosh, C. *et al.* 1q gain and CDT2 overexpression underlie an aggressive and highly proliferative form of Ewing sarcoma. *Oncogene* **31**, 1287–1298 (2012).

28. Kullendorff, C. M. *et al.* Cytogenetic aberrations in Ewing sarcoma: are secondary changes associated with clinical outcome? *Med. Pediatr. Oncol.* **32**, 79–83 (1999).

29. Musa, J. *et al.* Eukaryotic initiation factor 4E-binding protein 1 (4E-BP1): a master regulator of mRNA translation involved in tumorigenesis. *Oncogene* (2016) doi:10.1038/onc.2015.515.

30. Saxton, R. A. & Sabatini, D. M. mTOR Signaling in Growth, Metabolism, and Disease. *Cell* **168**, 960–976 (2017).

31. Goss, K. L. *et al.* The translational repressor 4E-BP1 regulates RRM2 levels and functions as a tumor suppressor in Ewing sarcoma tumors. *Oncogene* **40**, 564–577 (2021).

32. Morrison, C. Pfizer's CDK4/6 inhibitor approved for advanced breast cancer. *Nature Biotechnology* https://www-nature-com.emedien.ub.uni-muenchen.de/articles/nbt0415-323 (2015) doi:10.1038/nbt0415-323.

33. Asghar, U., Witkiewicz, A. K., Turner, N. C. & Knudsen, E. S. The history and future of targeting cyclin-dependent kinases in cancer therapy. *Nat. Rev. Drug Discov.* **14**, 130–146 (2015).

34. Sherr, C. J., Beach, D. & Shapiro, G. I. Targeting CDK4 and CDK6: From Discovery to Therapy. *Cancer Discov.* **6**, 353–367 (2016).

35. Mullard, A. FDA approves Novartis's CDK4/6 inhibitor. *Nat. Rev. Drug Discov.* **16**, 229–229 (2017).

36. van Tilburg, C. M. *et al.* The Pediatric Precision Oncology INFORM Registry: Clinical Outcome and Benefit for Patients with Very High-Evidence Targets. *Cancer Discov.* **11**, 2764–2779 (2021).

37. Garraway, L. A., Verweij, J. & Ballman, K. V. Precision oncology: an overview. *J. Clin. Oncol. Off. J. Am. Soc. Clin. Oncol.* **31**, 1803–1805 (2013).

38. Musa, J. & Grünewald, T. G. P. Interaction between somatic mutations and germline variants contributes to clinical heterogeneity in cancer. *Mol. Cell. Oncol.* **7**, 1682924 (2020).

39. Jahromi, M. S., Jones, K. B. & Schiffman, J. D. Copy Number Alterations and Methylation in Ewing's Sarcoma. *Sarcoma* **2011**, 362173 (2011).

40. Brisset, S. *et al.* CGH analysis of secondary genetic changes in Ewing tumors: correlation with metastatic disease in a series of 43 cases. *Cancer Genet. Cytogenet.* **130**, 57–61 (2001).

41. Ferreira, B. I. *et al.* Array CGH and gene-expression profiling reveals distinct genomic instability patterns associated with DNA repair and cell-cycle checkpoint pathways in Ewing's sarcoma. *Oncogene* **27**, 2084–2090 (2008).

42. Ozaki, T. *et al.* Genetic imbalances revealed by comparative genomic hybridization in Ewing tumors. *Genes. Chromosomes Cancer* **32**, 164–171 (2001).

43. Steiner, T. *et al.* Gain in Chromosome 8q Correlates with Early Progression in Hormonal Treated Prostate Cancer. *Eur. Urol.* **41**, 167–171 (2002).

44. Baykara, O., Bakir, B., Buyru, N., Kaynak, K. & Dalay, N. Amplification of Chromosome 8 Genes in Lung Cancer. *J. Cancer* **6**, 270–275 (2015).

45. Qin, L.-X. *et al.* The Association of Chromosome 8p Deletion and Tumor Metastasis in Human Hepatocellular Carcinoma1. *Cancer Res.* **59**, 5662–5665 (1999).

46. Mehrazin, R. *et al.* The correlation between gain of chromosome 8q and survival in patients with clear and papillary renal cell carcinoma. *Ther. Adv. Urol.* **10**, 3–10 (2018).

47. El Gammal, A. T. *et al.* Chromosome 8p deletions and 8q gains are associated with tumor progression and poor prognosis in prostate cancer. *Clin. Cancer Res. Off. J. Am. Assoc. Cancer Res.* **16**, 56–64 (2010).

48. Cai, Y. *et al.* Loss of Chromosome 8p Governs Tumor Progression and Drug Response by Altering Lipid Metabolism. *Cancer Cell* **29**, 751–766 (2016).

Funk *et al.*

49. Klatte, T. *et al.* Gain of chromosome 8q is associated with metastases and poor survival of patients with clear cell renal cell carcinoma. *Cancer* **118**, 5777–5782 (2012).

50. Hauffe, L. *et al.* Eukaryotic translation initiation factor 4E binding protein 1 (EIF4EBP1) expression in glioblastoma is driven by ETS1- and MYBL2-dependent transcriptional activation. *Cell Death Discov.* **8**, 91 (2022).

51. Guenther, L. M. *et al.* A Combination CDK4/6 and IGF1R Inhibitor Strategy for Ewing Sarcoma. *Clin. Cancer Res. Off. J. Am. Assoc. Cancer Res.* (2018) doi:10.1158/1078-0432.CCR-18-0372.

52. Shulman, D. S. *et al.* Phase 2 trial of palbociclib and ganitumab in patients with relapsed Ewing sarcoma. *Cancer Med.* **12**, 15207–15216 (2023).

53. Livak, K. J. & Schmittgen, T. D. Analysis of relative gene expression data using real-time quantitative PCR and the 2(-Delta Delta C(T)) Method. *Methods San Diego Calif* **25**, 402–408 (2001).

54. Wiederschain, D. *et al.* Single-vector inducible lentiviral RNAi system for oncology target validation. *Cell Cycle Georget. Tex* **8**, 498–504 (2009).

55. Marchetto, A. & Romero-Pérez, L. Western Blot Analysis in Ewing Sarcoma. *Methods Mol. Biol. Clifton NJ* **2226**, 15–25 (2021).

56. Funk, C. M. & Musa, J. Proliferation Assessment by Trypan Blue Exclusion in Ewing Sarcoma. *Methods Mol. Biol. Clifton NJ* **2226**, 151–158 (2021).

57. Schindelin, J. *et al.* Fiji: an open-source platform for biological-image analysis. *Nat. Methods* **9**, 676–682 (2012).

58. Schneider, C. A., Rasband, W. S. & Eliceiri, K. W. NIH Image to ImageJ: 25 years of image analysis. *Nat. Methods* **9**, 671–675 (2012).

59. Peterziel, H. *et al.* Drug sensitivity profiling of 3D tumor tissue cultures in the pediatric precision oncology program INFORM. *NPJ Precis. Oncol.* **6**, 94 (2022).

60. Berker, Y. *et al.* Patient-by-Patient Deep Transfer Learning for Drug-Response Profiling Using Confocal Fluorescence Microscopy of Pediatric Patient-Derived Tumor-Cell Spheroids. *IEEE Trans. Med. Imaging* **41**, 3981–3999 (2022).

61. ElHarouni, D. *et al.* iTReX: Interactive exploration of mono- and combination therapy dose response profiling data. *Pharmacol. Res.* **175**, 105996 (2022).

62. Cidre-Aranaz, F. & Ohmura, S. Tumor Growth Analysis of Ewing Sarcoma Cell Lines Using Subcutaneous Xenografts in Mice. *Methods Mol. Biol. Clifton NJ* **2226**, 191–199 (2021).

63. Koelsche, C. *et al.* Sarcoma classification by DNA methylation profiling. *Nat. Commun.* **12**, 498 (2021).

64. Franch-Expósito, S. *et al.* CNApp, a tool for the quantification of copy number alterations and integrative analysis revealing clinical implications. *eLife* **9**, e50267.

65. Colaprico, A. *et al.* TCGAbiolinks: an R/Bioconductor package for integrative analysis of TCGA data. *Nucleic Acids Res.* **44**, e71 (2016).

66. Therneau, T. M. & Grambsch, P. M. *Modeling Survival Data: Extending the Cox Model.* (Springer Science & Business Media, 2013).

67. Therneau, T. M., until 2009), T. L. (original S.->R port and R. maintainer, Elizabeth, A. & Cynthia, C. survival: Survival Analysis. (2023).

68. Stichel, D. *et al.* Routine RNA sequencing of formalin-fixed paraffin-embedded specimens in neuropathology diagnostics identifies diagnostically and therapeutically relevant gene fusions. *Acta Neuropathol. (Berl.)* **138**, 827–835 (2019).

69. McPherson, A. *et al.* deFuse: an algorithm for gene fusion discovery in tumor RNA-Seq data. *PLoS Comput. Biol.* **7**, e1001138 (2011).

70. Savola, S. *et al.* High Expression of Complement Component 5 (C5) at Tumor Site Associates with Superior Survival in Ewing's Sarcoma Family of Tumour Patients. *ISRN Oncol.* **2011**, 168712 (2011).

71. Postel-Vinay, S. *et al.* Common variants near TARDBP and EGR2 are associated with susceptibility to Ewing sarcoma. *Nat. Genet.* **44**, 323–327 (2012).

Funk *et al.*

72. Scotlandi, K. *et al.* Overcoming resistance to conventional drugs in Ewing sarcoma and identification of molecular predictors of outcome. *J. Clin. Oncol. Off. J. Am. Soc. Clin. Oncol.* **27**, 2209–2216 (2009).

73. Volchenboum, S. L. *et al.* Gene Expression Profiling of Ewing Sarcoma Tumors Reveals the Prognostic Importance of Tumor-Stromal Interactions: A Report from the Children's Oncology Group. *J. Pathol. Clin. Res.* **1**, 83–94 (2015).

74. Sannino, G. *et al.* Gene expression and immunohistochemical analyses identify SOX2 as major risk factor for overall survival and relapse in Ewing sarcoma patients. *EBioMedicine* **47**, 156–162 (2019).

75. Johnson, W. E., Li, C. & Rabinovic, A. Adjusting batch effects in microarray expression data using empirical Bayes methods. *Biostat. Oxf. Engl.* **8**, 118–127 (2007).

76. Yoshihara, K. *et al.* Inferring tumour purity and stromal and immune cell admixture from expression data. *Nat. Commun.* **4**, 2612 (2013).

77. Love, M. I., Huber, W. & Anders, S. Moderated estimation of fold change and dispersion for RNA-seq data with DESeq2. *Genome Biol.* **15**, 550 (2014).

78. Hothorn, T. maxstat: Maximally Selected Rank Statistics. (2017).

79. Korotkevich, G. *et al.* Fast gene set enrichment analysis. 060012 Preprint at https://doi.org/10.1101/060012 (2021).

80. Subramanian, A. *et al.* Gene set enrichment analysis: a knowledge-based approach for interpreting genome-wide expression profiles. *Proc. Natl. Acad. Sci. U. S. A.* **102**, 15545–15550 (2005).

81. Hänzelmann, S., Castelo, R. & Guinney, J. GSVA: gene set variation analysis for microarray and RNA-seq data. *BMC Bioinformatics* **14**, 7 (2013).

82. Barbie, D. A. *et al.* Systematic RNA interference reveals that oncogenic KRAS-driven cancers require TBK1. *Nature* **462**, 108–112 (2009).

83. Ritchie, M. E. *et al.* limma powers differential expression analyses for RNA-sequencing and microarray studies. *Nucleic Acids Res.* **43**, e47 (2015).

84. Ferrari, F., Solari, A., Battaglia, C. & Bicciato, S. PREDA: an R-package to identify regional variations in genomic data. *Bioinforma. Oxf. Engl.* **27**, 2446–2447 (2011).

85. Ge, S. X., Son, E. W. & Yao, R. iDEP: an integrated web application for differential expression and pathway analysis of RNA-Seq data. *BMC Bioinformatics* **19**, 534 (2018).

86. Waszak, S. M. *et al.* Germline Elongator mutations in Sonic Hedgehog medulloblastoma. *Nature* **580**, 396–401 (2020).

Funk *et al.*

FIGURES
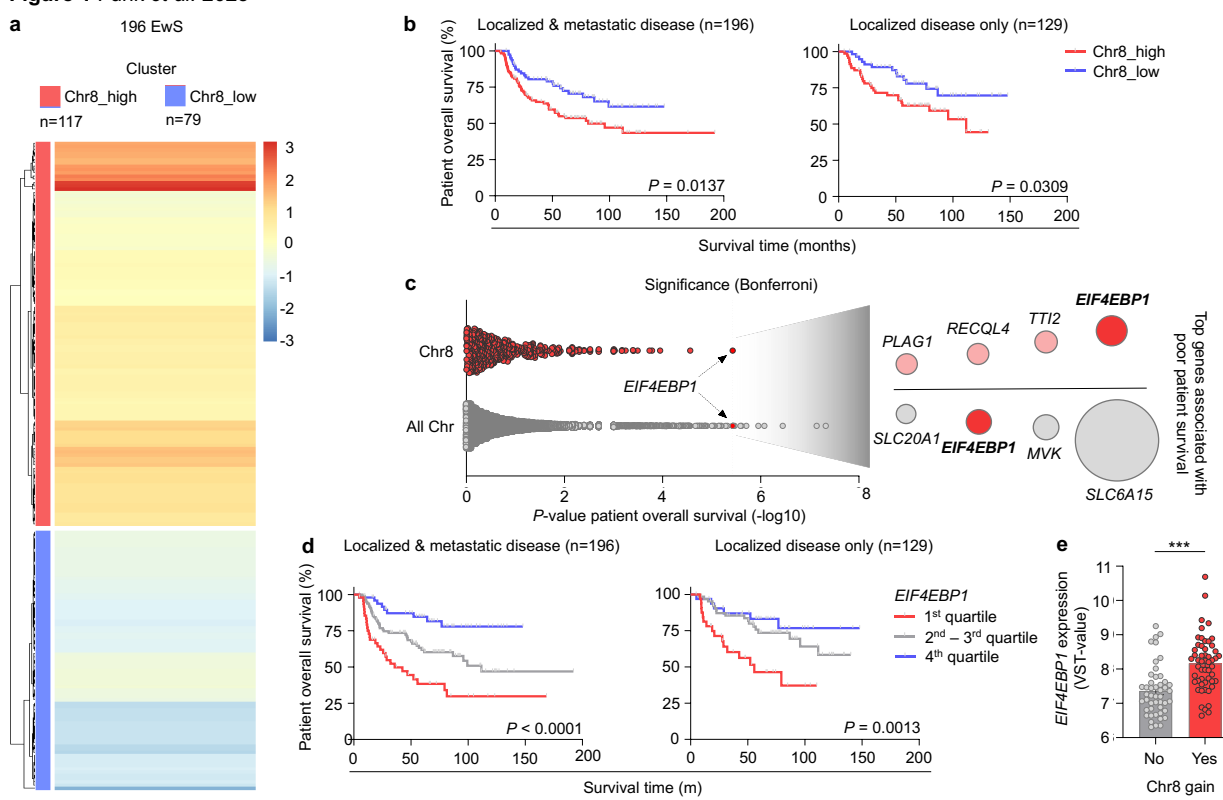
Figure 1: Chromosome 8 gain drives overexpression of the clinically relevant translation initiation factor 4E-BP1 in EwS. a Heat map showing 196 EwS patient tumors (Cohort 1) based on an inferred chr8 gene expression signature, assessed by single-sample Gene Set Enrichment Analysis (ssGSEA) followed by hierarchical clustering assigning each sample into either a high or low chr8 signature expression group. **b** Kaplan-Meier overall survival analysis of 196 EwS patients (Cohort 1) stratified into either a high or low chr8 signature expression group as described in (a). Kaplan-Meier plots are shown separately either for patients with localized & metastatic disease (n=196, left) or exclusively for patients with localized disease (n=129, right). *P*-values determined by Mantel-Haenszel test. **c** Overall survival batch analysis as assessed for every gene covered in transcriptomic profiling of 196 EwS patients (Cohort 1) using Mantel-Haenszel statistics. Chr8-located genes were additionally depicted separately. The dashed line indicates the Bonferroni-adjusted *P*-value threshold for significance. The dots on the right represent other genes reaching top statistical significance only for association with poor overall patient survival after Bonferroni correction next to *EIF4EBP1*. The dot size is negatively correlated with the *P* value of the respective gene. **d** Kaplan-Meier overall survival analysis of 196 EwS patients (Cohort 1) stratified by quartile *EIF4EBP1* expression. Kaplan-Meier plots are shown separately either for patients with localized & metastatic disease (n=196, left) or exclusively patients with localized disease (n=129, right). *P*-values determined by Mantel-Haenszel test. **e** *EIF4EBP1* expression as measured by RNA-seq in 100 primary EwS (Cohort 2) depending on the presence of chr8 gain as determined by methylation array. *P*-values determined by two-tailed Mann-Whitney test, horizontal bars represent means and whiskers represent the SEM. ***$P < 0.001$.

Funk *et al.*

Figure 2 Funk *et al.* 2023
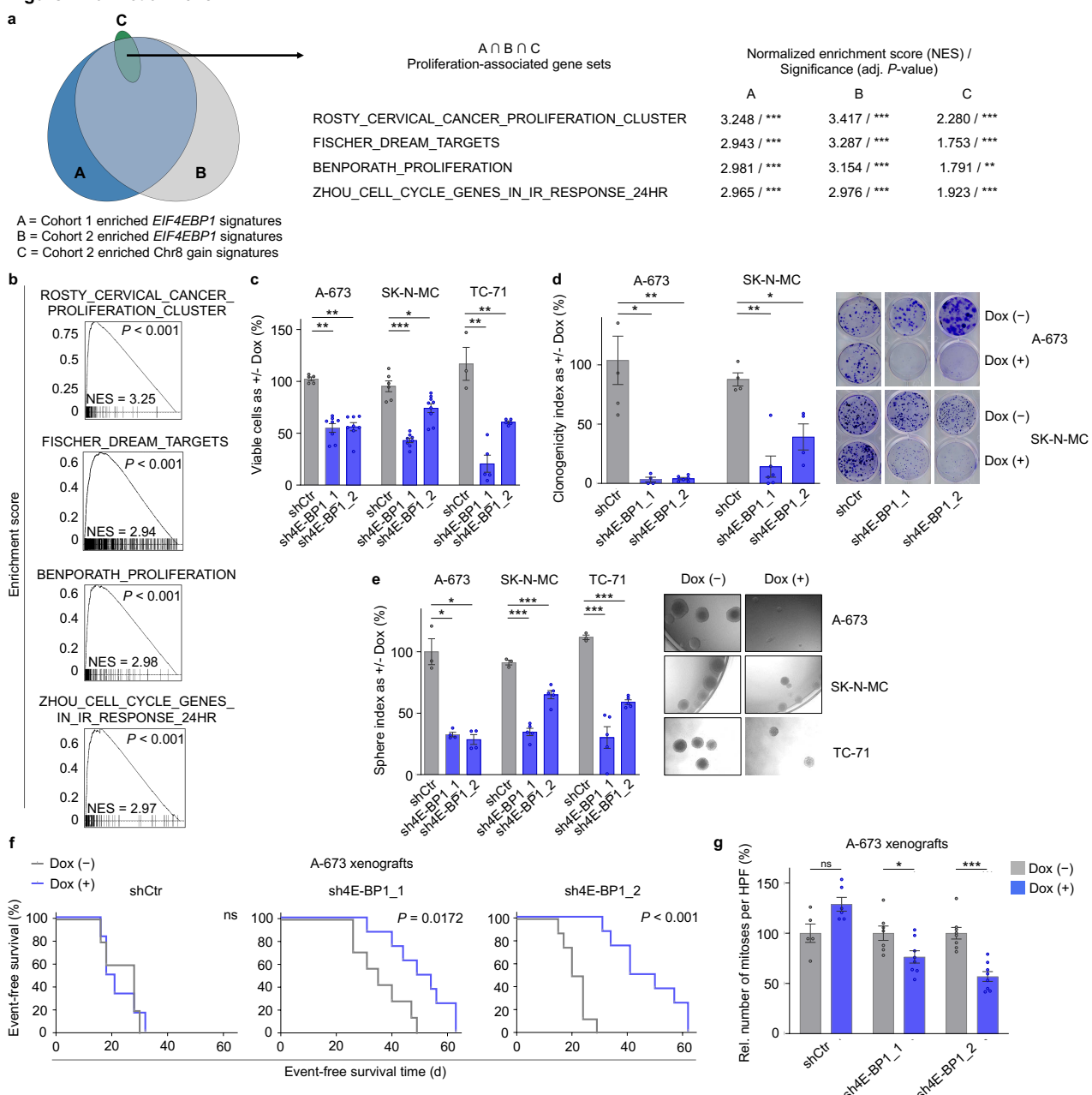
**Figure 2: High 4E-BP1 expression promotes EwS growth *in vitro* and *in vivo*. a** Area-proportional Venn diagram of gene sets enriched with *EIF4EBP1* expression in cohort 1 (A) and 2 (B) as well as with chr8 gain in cohort 2 (C) as determined by fGSEA. Exemplary gene sets representing a proliferation-associated enrichment signature in the overlap between A, B, and C are shown with respective normalized enrichment scores (NES) and significance levels. **b** fGSEA enrichment plots of exemplary gene sets given in (a). **c** Relative viable cell count of A-673, SK-N-MC, and TC-71 cells containing either Dox-inducible specific shRNA constructs directed against *EIF4EBP1* (sh4E-BP1_1 or sh4E-BP1_2) or a non-targeting shControl (shCtr). Cells were grown either with or without Dox for 120 h. Horizontal bars represent means, and whiskers represent the SEM, n≥4 biologically independent experiments. **d** Relative colony number of A-673 and SK-N-MC cells containing either Dox-inducible specific shRNA constructs directed against *EIF4EBP1* (sh4E-BP1_1 or sh4E-BP1_2) or a non-targeting shControl (shCtr). Cells were grown either with or without Dox for 8–14 d. Horizontal bars represent means, and whiskers the SEM, n≥4 biologically independent experiments. Representative images of colony formation are shown on the right.
e Sphere formation in A-673, SK-N-MC, and TC-71 cells containing shRNA constructs directed against *EIF4EBP1* (sh4E-BP1_1 or sh4E-BP1_2) or a non-targeting shControl (shCtr) treated with

37

Funk *et al.*

or without Dox for 8–14 d. Horizontal bars represent means, and whiskers represent the SEM, $n \geq 3$ biologically independent experiments. P-values determined by two-tailed unpaired t-test with Welch´s correction. Representative images of spheres are shown on the right. **f** Kaplan-Meier analysis of event-free survival of NSG mice xenografted with A-673 cells containing either Dox-inducible specific shRNA constructs directed against *EIF4EBP1* (sh4E-BP1_1 or sh4E-BP1_2) or a non-targeting shControl (shCtr). Once tumors were palpable, mice were randomized and treated with either vehicle (–) or Dox (+), $n \geq 5$ animals per condition. An 'event' was recorded when tumors reached a size maximum of 15 mm in one dimension. *P*-values determined via Mantel-Haenszel test. **g** Quantification of mitoses in HE-stained slides of xenografts described in (f). Five high-power fields (HPF) were counted per sample. Horizontal bars represent means, and whiskers represent the SEM, $n \geq 4$ samples per condition. ***$P < 0.001$, **$P < 0.01$, *$P < 0.05$, ns = not significant; *P*-values determined via two-tailed Mann-Whitney test if not otherwise specified.

Funk *et al.*

Figure 3 Funk *et al.* 2023
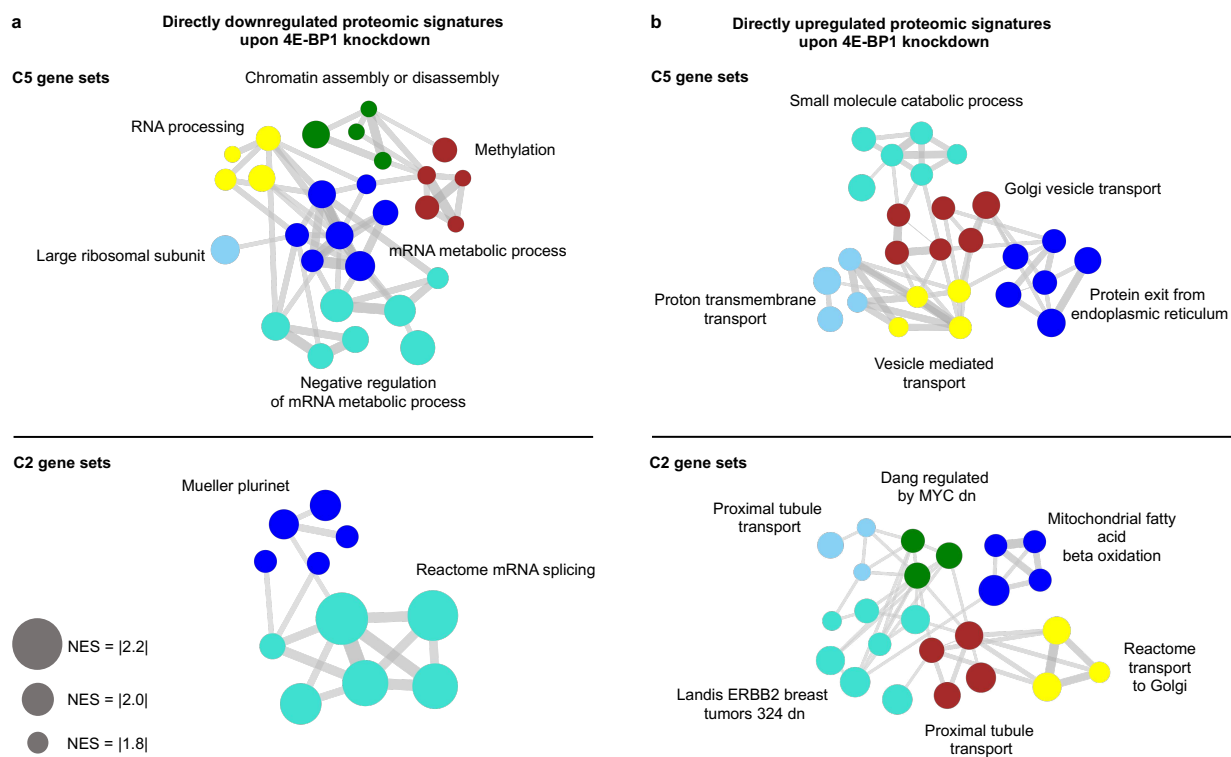
Figure 3: 4E-BP1 directly guides a multifunctional proteomic network. a Weighted Gene Correlation Network Analysis (WGCNA) depicting directly downregulated functional proteomic signatures upon 4E-BP1 knockdown considering C5 (upper) and C2 (lower) collections of gene sets of the Molecular Signatures Database (MSigDB). Network depicts signatures presenting *P*-values <0.05 and a normalized enrichment score (NES) >1.7. **b** WGCNA depicting directly upregulated functional proteomic signatures upon 4E-BP1 knockdown considering C5 (upper) and C2 (lower) collections of gene sets of the MSigDB. Network depicts signatures presenting *P*-values <0.05 and an NES < -1.7 and > 1.7. Line width of connection lines represents strength of interconnection between respective gene sets.

39

Funk *et al.*

Figure 4 Funk *et al.* 2023
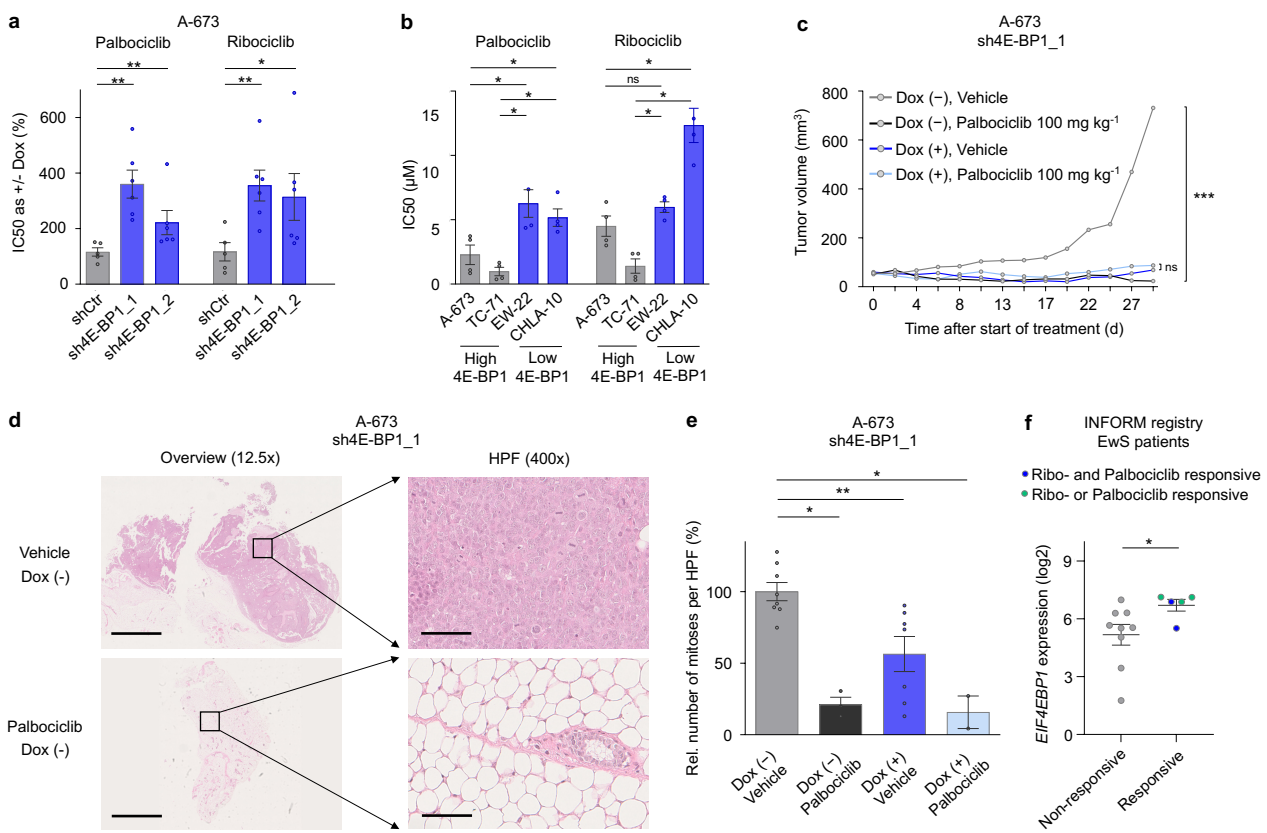
Figure 4: High 4E-BP1 expression sensitizes to targeted CDK4/6 inhibitor treatment with Palbociclib and Ribociclib.

a Analysis of IC50 of CDK4/6 inhibitors Palbociclib and Ribociclib in A-673 cells containing either DOX-inducible specific shRNAs directed against 4E-BP1 (sh4E-BP1_1, sh4E-BP1_2) or a non-targeting a non-targeting shControl (shCtr). Horizontal bars represent means, and whiskers represent the SEM, n≥5 biologically independent experiments **b** Analysis of IC50 of CDK4/6 inhibitors Palbociclib and Ribociclib in EwS cells with high (A-673, TC-71) and low (EW-22, CHLA-10) endogenous 4E-BP1 expression. Horizontal bars represent means, and whiskers represent the SEM, n≥3 biologically independent experiments. **c** NSG mice xenografted with A-673 EwS cells containing a Dox-inducible sh4E-BP1 construct, treated with/without Dox and either vehicle or Palbociclib in a dose of 100 mg/kg. Mice were randomized to the treatment groups when tumors were palpable. For each condition the mean tumor volume and SEM of 4–6 mice over the time of treatment are shown. HPF = high power field. **d** Representative HE stained micrographs of A673/sh4E-BP1 xenografts (DOX (–)) treated with either vehicle or Palbociclib as described in (c) (shown as an overview with 12.5× magnification and as a high-power field (HPF) in 400× magnification). Scale bar is 2.5 mm (12.5×) and 100 μm (400×). **e** Quantification of mitoses in micrographs of xenografts described in (c). Horizontal bars represent means, and whiskers represent the SEM, n≥2 samples per condition. **f** 3D drug sensitivity data with matched *EIF4EBP1* gene expression data from 14 EwS patient tumor cell cultures treated within the INFORM registry either with Palbociclib or Ribociclib. ***$P < 0.001$, **$P < 0.01$, *$P < 0.05$, ns = not significant; P-values determined via two-tailed Mann-Whitney test if not otherwise specified.

Funk *et al.*

Supplementary Figure 1 Funk *et al.* 2023
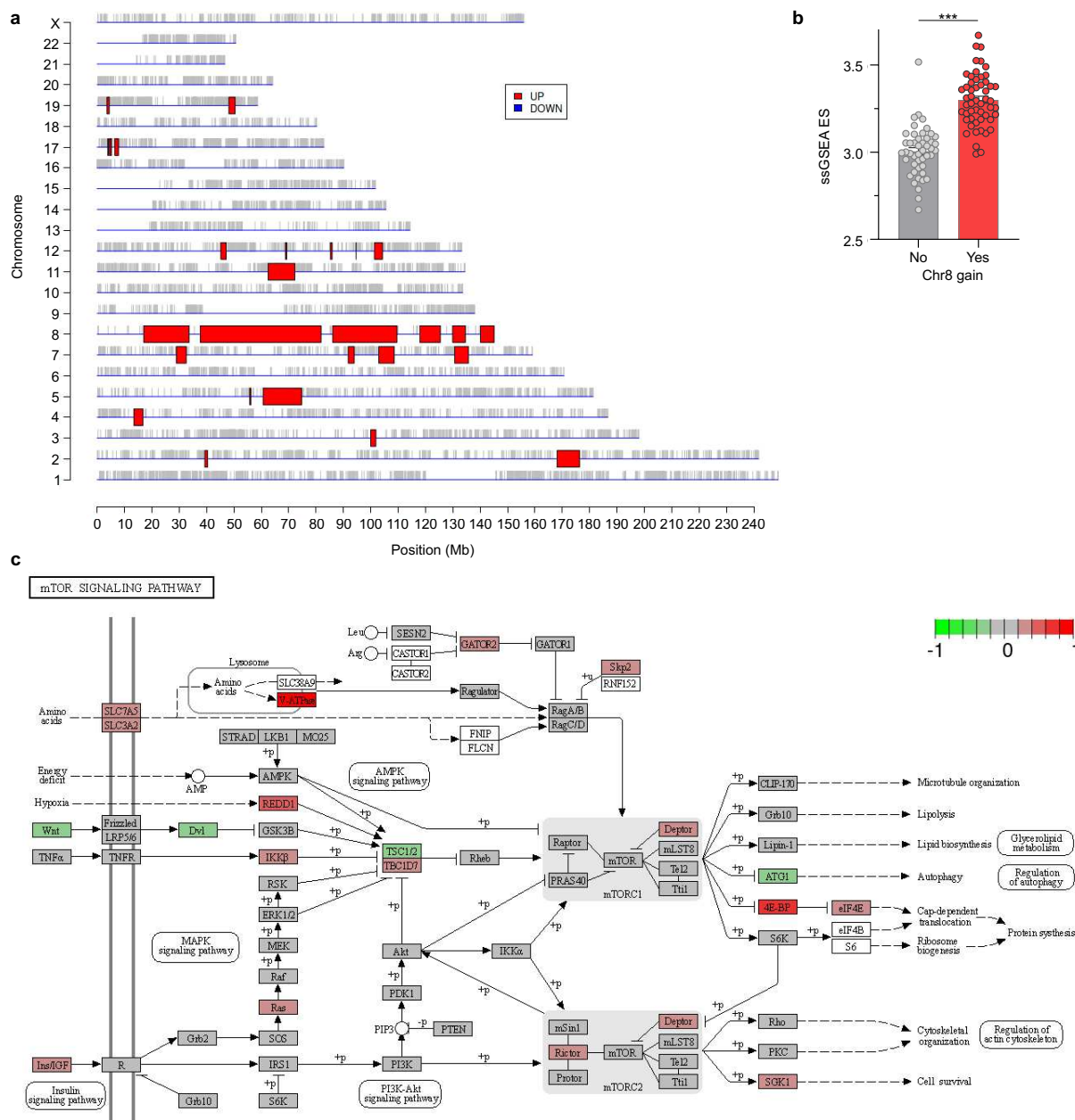
Supplementary Figure 1: Model validation, chromosomal location, and mTOR pathway representation of genes differentially upregulated in the chr8 high gene expression signature group in EwS.

a Differentially expressed genes (DEGs) between chr8 high and low gene expression cluster mapped onto chromosomes using Position Related Data Analysis (PREDA). **b** ssGSEA enrichment scores for high chr8 gene expression signature as measured by RNA-seq in 100 primary EwS (Cohort 2) depending on the presence of chr8 gain as determined by methylation array. **c** DEGs between chr8 high and low gene expression within the mTOR signaling pathway. ***$P < 0.001$, P-values determined via two-tailed Mann-Whitney test.

Funk *et al.*

Supplementary Figure 2 Funk *et al.* 2023
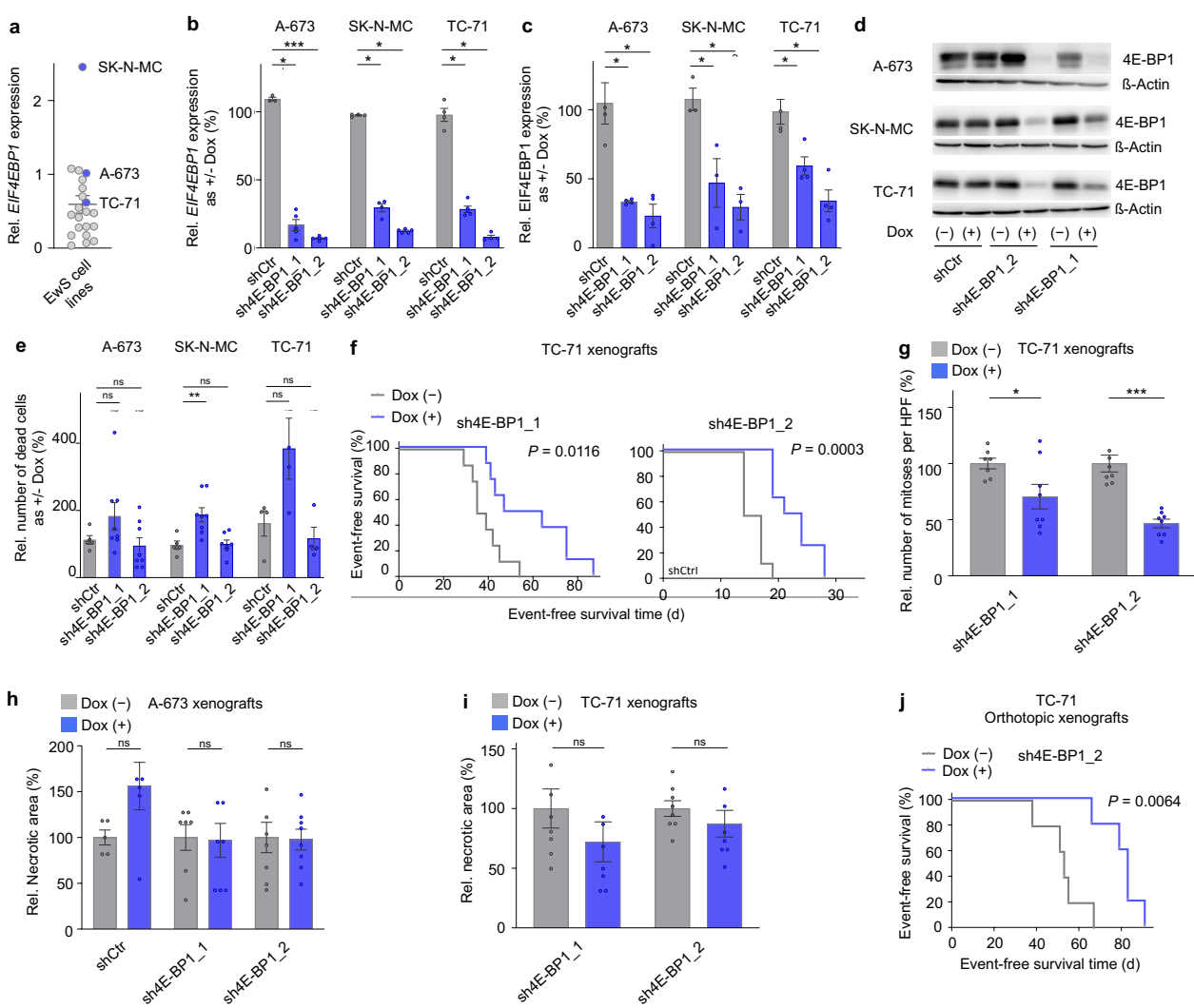
Supplementary Figure 2: RNAi-mediated knockdown of 4E-BP1 inhibits EwS growth.
a Relative *EIF4EBP1* expression in 21 wildtype EwS cell lines as determined by qRT-PCR. *EIF4EBP1* expression of each cell line is normalized to that of A-673. **b** Relative *EIF4EBP1* expression as assessed by qRT-PCR in A-673, SK-N-MC, and TC-71 cells containing either Dox-inducible specific shRNA constructs directed against *EIF4EBP1* (sh4E-BP1_1 or sh4E-BP1_2) or a non-targeting shControl (shCtr). Cells were grown either with or without Dox for 96 h. Horizontal bars represent means, and whiskers represent the SEM, n≥3 biologically independent experiments. **c** Relative 4E-BP1 expression as assessed by quantified western blotting in A-673, SK-N-MC, and TC-71 cells containing either Dox-inducible specific shRNA constructs directed against *EIF4EBP1* (sh4E-BP1_1 or sh4E-BP1_2) or a non-targeting shControl (shCtr). Cells were grown either with or without Dox for 96 h. *P*-values determined via one-tailed Mantel-Haenszel test. **d** Representative western blots as described in (c) are shown. ß-actin served as a loading control. **e** Relative number of dead cells as assessed by Trypan blue exclusion in A-673, SK-N-MC, and TC-71 cells containing either Dox-inducible specific shRNA constructs directed against *EIF4EBP1* (sh4E-BP1_1 or sh4E-BP1_2) or a non-targeting shControl (shCtr). Cells were grown either with or without Dox for 96 h. Horizontal bars represent means, and whiskers represent the SEM, n≥4 biologically independent experiments. **f** Kaplan-Meier analysis of event-free survival of NSG mice xenografted with TC-71 cells containing Dox-inducible specific shRNA constructs directed against *EIF4EBP1* (sh4E-BP1_1 or sh4E-BP1_2). Once tumors were palpable, mice were randomized and treated with either vehicle (–) or Dox (+), n =8 animals per condition. An 'event' was recorded when tumors reached a size

Funk *et al.*

maximum of 15 mm in one dimension. *P*-values determined via Mantel-Haenszel test. **g** Quantification of mitoses in HE-stained slides of xenografts described in (f). Five high-power fields (HPF) were counted per sample. Horizontal bars represent means, and whiskers represent the SEM, $n \geq 7$ samples per condition. **h** Quantification of necrotic area on HE-stained slides of A-673 xenografts described in (f). Five high-power fields (HPF) were analyzed per sample. Horizontal bars represent means, and whiskers represent the SEM, $n \geq 5$ samples per condition. **i** Quantification of necrotic area on HE-stained slides of TC-71 xenografts described in (f). Five high-power fields (HPF) were analyzed per sample. Horizontal bars represent means, and whiskers represent the SEM, $n \geq 7$ samples per condition. **j** Kaplan-Meier analysis of event-free survival of NSG mice orthotopically xenografted into the proximal tibia with TC-71 containing a Dox-inducible specific shRNA construct directed against *EIF4EBP1* (sh4E-BP1_2). One day after injection of the cells, mice were randomized and treated with either vehicle (–) or Dox (+), $n = 5$ animals per condition. An 'event' is recorded when the mice exhibited signs of limping at the injected leg. *P*-values determined via Mantel-Haenszel test. ***$P < 0.001$, **$P < 0.01$, *$P < 0.05$, ns = not significant; *P*-values determined via two-tailed Mann-Whitney test if not otherwise specified.

Funk *et al.*

Supplementary Figure 3 Funk *et al.* 2023
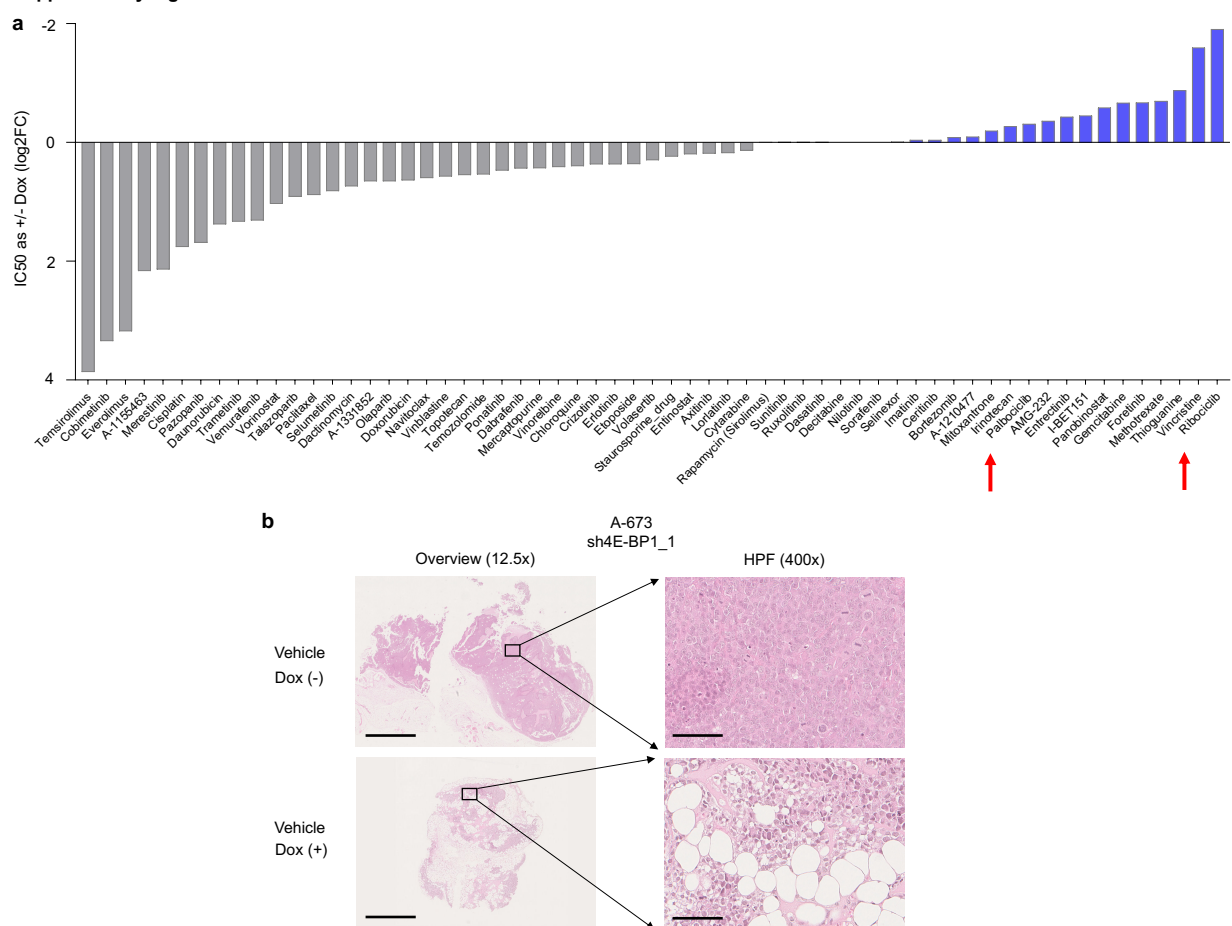
Supplementary Figure 3: High 4E-BP1 expression specifically sensitizes for targeted CDK4/6 inhibitor treatment. a 3D drug screening data of A-673 EwS cells constituting a Dox-inducible shRNA directed against 4E-BP1 and treated with/without Dox and respective indicated inhibitors in serially increasing concentrations. **b** Analysis of IC50 of Vincristine, Thioguanine, Methotrexate, Gemcitabine in A-673 cells containing either Dox-inducible specific shRNAs directed against 4E-BP1 (sh4E-BP1_1, sh4E-BP1_2) or a non-targeting shControl construct. Horizontal bars represent means, and whiskers represent the SEM, n≥3 biologically independent experiments. **c** Representative HE stained micrographs of A673/sh4E-BP1 xenografts treated either with or without Dox (shown as an overview with 12.5× magnification and as a high-power field (HPF) in 400× magnification). Scale bar is 2.5 mm (12.5×) and 100 μm (400×). HPF = high power field. ns = not significant; *P*-values determined via two-tailed Mann-Whitney test if not otherwise specified.

Funk *et al.*

Supplementary Figure 4 Funk *et al.* 2023
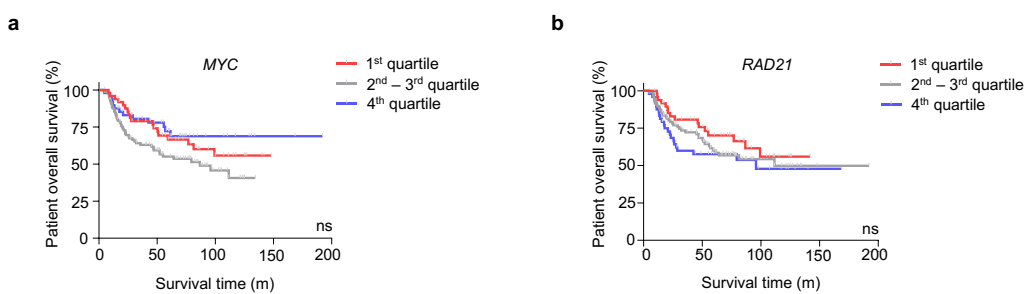
Supplementary Figure 4: Kaplan-Maier survival analysis in Cohort 1 stratifying patients by quartile *MYC* and *RAD21* expression. a Kaplan-Meier overall survival analysis of 196 EwS patients (Cohort 1) stratified by quartile *MYC* expression. **b** Kaplan-Meier overall survival analysis of 196 EwS patients (Cohort 1) stratified by quartile *RAD21* expression. *P*-values determined by Mantel-Haenszel test. ns = not significant.